Reviews in Mineralogy & Geochemistry
Vol. 89 pp. 787-827, 2023
Copyright © Mineralogical Society of America

Surface Volatiles on the Moon

Dana M. Hurley[1], Matthew A. Siegler[2], Joshua T. S. Cahill[1], Anthony Colaprete[3], Emily Costello[4], Ariel N. Deutsch[3], Richard C. Elphic[3], Wenzhe Fa[5], Cesare Grava[6], Paul O. Hayne[7], Jennifer Heldmann[3], Amanda R. Hendrix[2], Andrew P. Jordan[8], Rosemary M. Killen[9], Rachel L. Klima[1], Georgiana Kramer[2], Shuai Li[4], Yang Liu[10], Paul G. Lucey[4], Erwan Mazarico[9], Yvonne Pendleton[3], Michael Poston[6], Parvathy Prem[1], Kurt D. Retherford[6], Micah Schaible[11]

[1]Johns Hopkins University Applied Physics Laboratory, 11100 Johns Hopkins Road, Laurel, Maryland 20723, U.S.A.
dana.hurley@jhuapl.edu, joshua.cahill@jhuapl.edu, rachel.klima@jhuapl.edu, parvathy.prem@jhuapl.edu

[2]Planetary Science Institute, 1700 E Fort Lowell Rd STE 106 Tucson, Arizona 85719, U.S.A.
msiegler@psi.edu, ahendrix@psi.edu, gkramer@psi.edu

[3]NASA Ames Research Center, Moffett Field, California 94035, U.S.A.
anthony.colaprete-1@nasa.gov, ariel.deutsch@nasa.gov, richard.c.elphic@nasa.gov, jennifer.heldmann@nasa.gov, pendletonyvonne@gmail.com

[4]Hawai'i Institute of Geophysics and Planetology, University of Hawaii at Manoa, Honolulu, Hawai'i 96822, U.S.A.
ecostello@higp.hawaii.edu, shuaili@hawaii.edu, lucey@higp.hawaii.edu

[5]Institute of Remote Sensing and GIS, Peking University, Beijing 100871, China
wzfa@pku.edu.cn

[6]Southwest Research Institute, 220 Culebra Road, San Antonio, Texas 78238, U.S.A.
cesare.grava@swri.org, michael.poston@swri.org, kretherford@swri.edu

[7]Astrophysical and Planetary Sciences, 2000 Colorado Avenue, University of Colorado, Boulder, Colorado 80309, U.S.A.
paul.hayne@colorado.edu

[8]Institute for the Study of Earth, Oceans, and Space, University of New Hampshire Morse Hall, 8 College Road, Durham, New Hampshire 03824, U.S.A.
a.p.jordan@unh.edu

[9]NASA Goddard Space Flight Center, 800 Greenbelt Rd, Greenbelt, Maryland 20771, U.S.A.
rosemary.killen@nasa.gov, erwan.m.mazarico@nasa.gov

[10]National Space Science Center, Zhongguancun Nanertiao 1, Beijing, 100190, China
yangliu@nssc.ac.cn

[11]School of Chemistry and Biochemistry, Georgia Institute of Technology Atlanta, Georgia 30332, U.S.A.
mjschaible@gatech.edu

1529-6466/23/0089-0018$05.00 (print)
1943-2666/23/0089-0018$05.00 (online)
http://dx.doi.org/10.2138/rmg.2023.89.18

1. INTRODUCTION

Discovery of water in lunar samples and on the lunar surface has opened a new chapter in lunar exploration. In addition to their potential utility, water and other volatile compounds can record a vast amount of information about the evolution of the Moon and migration of material throughout the Solar System. This chapter centers on volatile species (H_2O, OH, CO_2, Ar, etc.) identified and theorized in the upper microns to meters of the lunar surface. While volatiles are generally thought of as residing within the cold, permanently shadowed regions (PSR) near the lunar poles, volatiles also occur globally (Fig. 1). Their mobility, concentration, and spatial expanse are currently the subject of great debate within the community.

Understanding surface volatiles and their origins requires investigation of sources, transformations via chemical reactions, physical mobility, sequestration, and loss processes. Remote sensing techniques spanning spectroscopy, particle physics, and radar/lidar combine to provide multiple viewpoints of the presence of volatiles (see Gaddis et al. 2023, this volume). Currently, some of these data appear contradictory with each other. In addition, critical information for understanding volatile lifetimes and mobility on the lunar surface comes from lunar sample analysis, surface temperature measurements, exosphere measurements, laboratory experiments, and mathematical modeling. Here, we summarize recent advances.

Each technique used to examine lunar surface volatiles is sensitive to different volatile species, states, and related products (i.e., hydrogen versus hydroxyl versus isolated water molecules versus decimeter-scale deposits of water-ice) and differing scales and depths within the lunar surface. Consequently, some techniques are most sensitive to volatiles adsorbed to the surfaces of lunar grains, while others may be dominated by bulk properties. As surface species are more prone towards migration and/or loss than are volatiles trapped in a grain, each technique may be sensitive to a different source/sink of volatiles. As such, some techniques should compare well with measurements from lunar samples (see McCubbin et al. 2023, this volume), while others will be more relevant as sources to the lunar exosphere (see Farrell et al. 2023, this volume).

Ultimately, volatiles are sought after for primarily two reasons: 1) the information they provide regarding the history of the Moon, which in turn provides a wealth of information about the history of the Earth, and indeed the entire Solar System; and 2) to be used as a resource for further exploration of the Moon and beyond, including exploration by humans (see Crawford et al. 2023, this volume).

We start by summarizing what was known about lunar volatiles before the modern re-awakening of volatile investigation in the mid 2000's. Next, we present the current understanding of volatile form, distribution, and abundance on the Moon. Following that we discuss the dynamic lifecycle(s) of volatiles on the Moon. Finally, we conclude by describing the most pressing outstanding questions for understanding volatiles on the Moon and relate to other relevant bodies, such as asteroids and Mercury.

1.1. Definition of volatiles

Volatiles are molecules that are typically found in the gas phase of matter on Earth's surface. This definition varies depending on the temperature, gravity, and atmosphere of a body. We therefore define volatiles in reference to the Moon itself, an airless body at ~1 AU from the Sun. Here we will take "volatiles" to mean molecules that cannot remain on the lunar surface in direct sunlight at the lunar equator, where temperatures can exceed 400 K. However, there are degrees of volatility inherent within this definition because there is a wide range of temperatures on the Moon. Volatile species on the Moon include, most notably, water (H_2O), hydroxyl (OH^-), CO_2, Ar, He, Ne, SO_2, S, NH_3, Na, K, H_2, CH_4 and a large host of organic hydrocarbons.

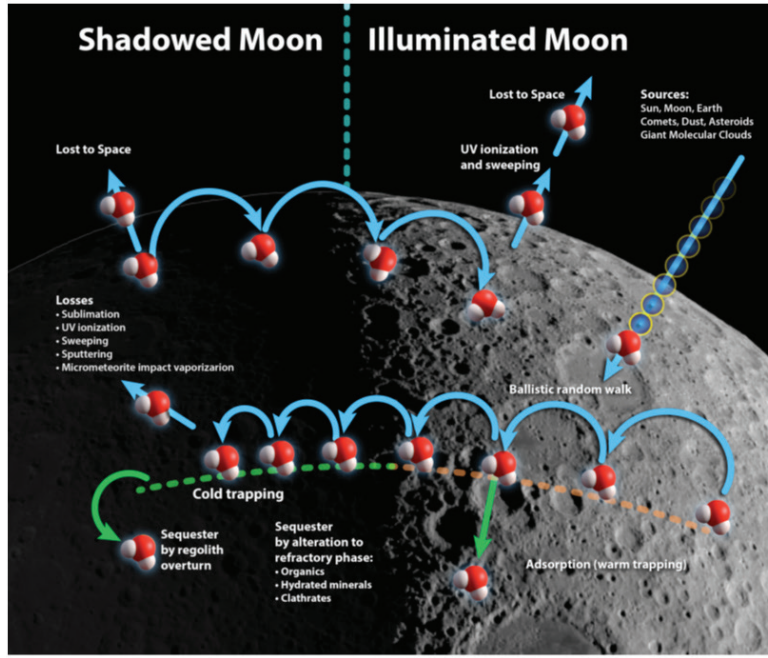

Figure 1. Sources, transport, and sinks of lunar volatiles. [Used by permission of Keck Institute for Space Studies © 2014 from Hayne et al. (2013).] Adapted from Lucey (2009).

A practical way to characterize volatiles is by a residence time on the surface. This residence time can be affected both by temperature, which controls the energy a molecule has to leave a surface, and binding energy to that surface. Figure 2 shows the nominal stability temperature of many volatile constituents of the Moon (Zhang and Paige 2009). Some volatiles are relatively stable in the cold PSR, but not in regions that receive some direct sunlight. These often temporarily adsorb to the surface on the nightside but are released into the exosphere on the dayside, such as Ar. The range of volatility temperatures for different molecules provides a mechanism to study gas-surface interactions on the Moon. The least volatile extreme are species like Na, K, and OH which are thermally stable everywhere on the Moon, but are released from the surface by energetic processes. The PSRs, being the coldest locations on the Moon, act as a reservoir for any of the volatiles that can condense or adsorb with long residence times. The most volatile species, such as He, H_2, and Ne, cannot reside for long periods of time anywhere on the Moon's surface, and thus mainly exist as exospheric species.

1.2. Old view of volatiles and recent developments

After Apollo, the Moon was considered dry, devoid of water and most volatiles. This is evident in that the last edition of "New Views" did not even include a volatiles section. The lack of volatiles was a driving constraint in the development of the currently accepted theory for how the Moon formed (Hartmann and Davis 1975; Nakajima and Stevenson 2018). Water that had been found in lunar samples was assumed primarily to be contamination from the inevitable encounter with volatile species in the process of returning these samples to Earth (Epstein and Taylor 1970). The concentration and isotopic composition of hydrogen, carbon and silicon in Apollo 11 lunar rocks and minerals were correlated with the surface indicating that lunar rocks were anhydrous (DesMarais et al. 1974). The surface of returned regolith grains was found to be highly reactive with plentiful sites for water and other species to bond (Holmes et al. 1973). The "seas" of the Moon were dry.

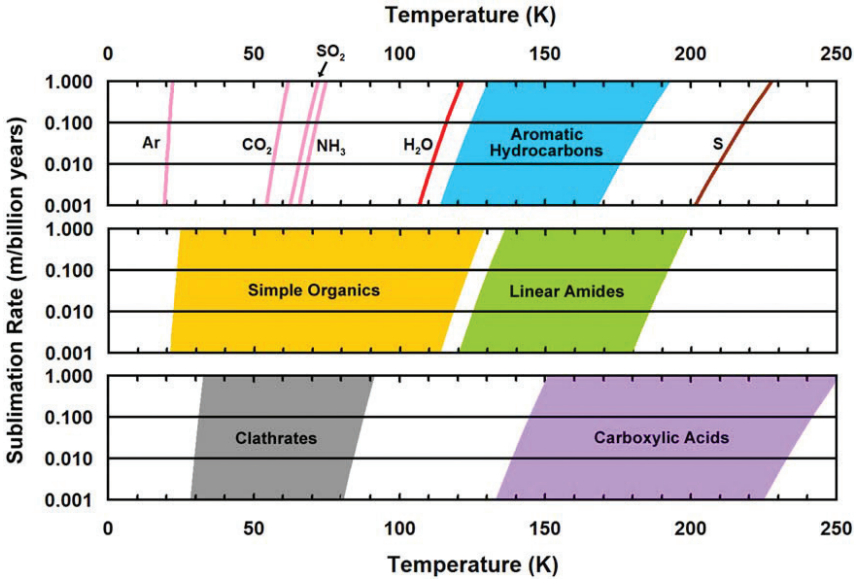

Figure 2. Nominal sublimation rates of plausible lunar volatiles as a function of temperature. [Reproduced with permission of John Wiley & Sons Ltd from Zhang JA, Paige DA (2009) Cold-trapped organic compounds at the poles of the Moon and Mercury: Implications for origins. Geophys Res Lett 36:L16203 © 2009 American Geophysical Union]

The poles were always the potential exception. The survival of water ice in shadowed polar craters was suggested by Urey (1952) and first examined in detail by Watson et al. (1961). Due to the small angle between the lunar spin axis and the ecliptic normal (1.54°), surface temperatures within polar craters can remain cold enough to prevent substantial loss of ice by sublimation (Arnold 1979). At temperatures below approximately 110 K, sublimation of exposed water ice will slow to less than 1 m per billion years (Watson et al. 1961; Schorghofer and Taylor 2007). However, a lack of new data and apparent lack of volatiles in returned Apollo samples led to little study on this topic.

The discovery of apparent water ice deposits at the poles of Mercury (Paige 1992; Slade et al. 1992), which has now been confirmed (Lawrence et al. 2013; Paige et al. 2013; Lawrence 2017), reopened interest in the potential of polar volatiles on the Moon (Vasavada et al. 1999). Potential detection of water ice on the Moon by the Clementine radar (Nozette et al. 1996) was initially questioned (Stacy et al. 1997) and has not held up to further scrutiny (Margot et al. 1999; Simpson and Tyler 1999; Campbell et al. 2006).

LPNS measurements, which are sensitive to much smaller concentrations than radar have seen evidence of polar hydrogen (e.g., Feldman et al. 1998, 2000; Eke et al. 2009; Miller et al. 2014). This result has been advanced by the LRO LEND instrument (e.g., Sanin et al. 2017). While these hydrogen detections generally coincide with the lunar cold traps, it has yet to be confirmed whether these are water ice or some form of chemically bound hydrated minerals.

The discovery of hydrogen rich deposits in the polar regions helped motivate renewed laboratory studies. Saal et al. (2008) found the first clear evidence of indigenous lunar water within lunar glasses. Subsequent studies have found evidence for water and other volatiles in returned samples (Boyce et al. 2010; Saal et al. 2013) that may serve as a source of global surface volatiles. These internal volatiles are covered in McCubbin et al. (2023, this volume)

Near-infrared data from Chandrayaan-1, Cassini, and Deep Impact/EPOXI indicated near-global spectral absorptions consistent with the presence of water and hydroxyl on the sunlit

surface of the Moon (Clark 2009; Pieters et al. 2009; Sunshine et al. 2009). These data require a careful correction for the effects of thermal infrared wavelengths. Multiple correction techniques have been applied and have led to varying estimates on total volatile concentration (Li and Milliken 2016; Bandfield et al. 2017). LRO observations in the UV (Gladstone et al. 2012; Hayne et al. 2015), LOLA laser reflectance measurements (Fisher et al. 2017), and near-infrared spectra (Li et al. 2018) show various possible detections of surface water features within the PSRs.

The most direct evidence for polar volatiles comes from the LCROSS (Lunar Crater Observation and Sensing Satellite) mission, which impacted into the PSR of Cabeus crater near the lunar south pole and detected water ice in the lunar regolith (Colaprete et al. 2010). Analysis of lunar materials lofted into the impact plume further demonstrated the presence of water ice molecules which sublimated and photo-dissociated after reaching sunlight (Heldmann et al. 2015).

1.3. Significance of volatiles

The Moon provides a witness plate for the supply of volatiles to the Earth. The polar cold traps of the Moon could potentially harbor very ancient volatiles which could hold a long-term record of the delivery of material to the Moon (Arnold 1979; Siegler et al. 2015, 2016), either from external sources (comets, solar wind, asteroids, micrometeorites, etc.) or outgassing from the lunar interior (e.g., Needham and Kring 2017). Much as the cratering record of the Moon preserves a bombardment record lost on the Earth, lunar volatiles may serve as a unique record of delivery of external water and other compounds to the Earth. If volatiles are found to have been outgassed from the interior, they may play a substantial role in interior rheologic processes and help constrain models of lunar origin.

While the Moon is not believed to have ever been capable of harboring life (Matthewman et al. 2015), comparison of lunar volatiles with other volatile deposits in the inner solar system (e.g., Mercury, Mars, NEAs) may enhance understanding of planetary habitability. As water is believed to be the key element required for life, the record of how and when it was delivered to the Earth is critical in our understanding of how Earth itself became habitable. Future human presence on the Moon is also heavily reliant on our ability to use in-situ resources, as discussed by Crawford et al. (2023, this volume). In-situ resource utilization (ISRU) of volatiles is an important component of future exploration because the ability to extract and process key resources can significantly reduce the required launch mass, risk, and cost of human and robotic space exploration (Sanders and Larsen 2015; Carpenter et al. 2016). Some of these uses include propellants, life support, power system consumables, and radiation and rocket exhaust shielding.

1.4. Reservoirs of volatiles

The permanently (or more accurately, persistently, as long-term polar orientation has changed) shadowed regions of the Moon have long been postulated to be the largest volatile reservoir on the Moon (Urey 1952; Watson et al. 1961; Arnold 1979). These regions have now been extensively mapped by LRO, Kaguya, and other missions, with boundaries defined by temperature (e.g., Siegler et al. 2015), or shadow from direct sunlight (Gläser et al. 2018).

Reservoirs of volatiles exist on several scales, ranging from volatiles incorporated inside lunar grains (e.g., Hashizume et al. 2000; Saal et al. 2008; Greenwood et al. 2011; Liu et al. 2012; McCubbin et al. 2015), adsorbed to lunar grain surfaces (e.g., Cocks et al. 2002; Goering et al. 2008; Hibbitts 2011; Poston 2013, 2015), and condensed in cryogenically-cold locations (e.g., Colaprete et al. 2010; Paige et al. 2010). Each volatile species will have its own behavior of trapping, adsorption, and condensation. Condensed volatiles are stable only in PSRs, while internal and strongly adsorbed volatiles can persist in warmer locations.

The most obvious PSRs are large craters near the lunar poles, which due to the small lunar obliquity (with respect to the Sun) have not seen direct sunlight in millions to billions of years (possibly never at all). However, PSRs too small to resolve in current data have

been suggested and could also serve as long-term condensation locations for volatiles. These "micro-coldtraps" (e.g., McGovern et al. 2013; Hayne and Aharonson 2015; Rubanenko and Aharonson 2017) are likely to exist down to scales of 10's of cm and could exist poleward of ~75° latitude, but the stability of ice is highly dependent on the depth to diameter ratio of small craters and surface roughness (Vasavada et al. 1999).

Water ice will last on the surface of the Moon for about a billion years if it remains at $\lesssim$ 110 K (Watson et al. 1961; Schorghofer and Taylor 2007; Siegler et al. 2011). The Moon has about 26,000 km^2 of surface area in the large shadowed regions near the poles cold enough for surface ice to be stable (Paige et al. 2010; Mazarico et al. 2011; Siegler et al. 2016). However, due to the insulating nature of lunar dust, ice buried by as little as 10 cm can survive surface temperatures up to 125 K for billions of years (Schorghofer and Taylor 2007). In porous material, most heat is transferred via the gasses in pore spaces. Therefore, regolith under vacuum is one of the greatest thermal insulators in the universe, with thermal conductivities below 10^{-3} W·m^{-1}·K^{-1}. This prevents short periods of maximum heating from reaching depth. Lunar grains are also highly irregular, making a very tortuous path for molecules migrating through the regolith. The Moon has 240,000 km^2 of area in the upper meter alone that could harbor subsurface ice (at 1% filling fraction this would be 2.4 km^3, or about 3 times the volume of Halley's comet). Depending on how deep ice could be buried, and how it initially arrived to the Moon, volumes of ice could be much greater.

Adsorbed volatiles will be stable anywhere condensed volatiles are stable, but can also be retained in relatively cool locations, such as locations that only receive a small amount of sunlight each lunar day. Lunar samples collected from such locations showed enhanced content of volatiles, such as mercury (Hg). Likewise, methane (CH_4) discovered in the LCROSS plume should not be stable even at low temperatures (Paige et al. 2010), but was observed (Colaprete et al. 2010), hinting that surface adsorption could be responsible.

Internal volatiles could theoretically have been trapped since the formation of the Moon. The best examples of such volatile reservoirs are pyroclastic deposits (Klima et al. 2013; Klima and Petro 2017). However, internal volatiles also include implanted solar wind particles, which have been shown to be concentrated near the surfaces of lunar grains (DesMarais et al. 1974; Hashizume et al. 2000). In many cases, detections of volatiles by remote sensing likely represent a superposition of all reservoirs.

There is no reason that the deeper subsurface (~5 m to 1 km) should be devoid of water ice and other volatiles that have currently evaded detection. Temperatures in the subsurface can be cool enough that water ice would sublimate at a negligible rate; and it is not unreasonable that some pore space exists to these depths (Besserer et al. 2014). Assumptions as to how ice would get to such depths, be it by impact burial, being driven downward by a past episode of warmer temperatures at high obliquity (e.g., Paige et al. 2010; Siegler et al. 2011, 2015, 2016), or perhaps outgassing from the lunar interior are speculative at present.

2. QUANTIFYING PRESENT DAY VOLATILES

Many measurements of volatiles on the surface of the Moon have been made, especially since the Lunar Prospector mission. This section reports the measurements of surface volatiles in terms of the abundance, composition, distribution, and physical form of the volatiles. The abundance is the absolute quantity of volatiles that are present. Composition refers to the molecular species that comprise the lunar volatiles. The distribution is the spatial and temporal variations in the volatile contents. This is separated out from the concept of the physical form, which means whether, for example, a water molecule is adsorbed to a regolith grain surface, exists as a frost, is part of an ice coating on a grain, or is part of a coherent, pure block of ice.

Although a rough idea of abundance and distribution existed from the Lunar Prospector neutron data in 2000, much progress has been made in understanding since then. Likewise, knowledge of the composition and the physical form of volatiles has gone through paradigm shifts since the early 2000s. In fact, the highly complementary data from multiple missions and measurement techniques provide great insight into these factors. These measurements are presented separately for the volatiles within the PSR and those distributed more globally on the surface of the Moon.

2.1. Abundance

2.1.1. Permanently shadowed regions. From Lunar Prospector, a general picture of the abundance of H-bearing material in the top 1-m of lunar regolith emerged. As shown in Figure 3, the Lunar Prospector Neutron Spectrometer (LPNS) measurements are consistent with an increased abundance of H at latitudes poleward of 75°. The average abundance of hydrogen in the polar regions is estimated to be about 100 ppm or ~0.1 wt.% water-equivalent hydrogen (WEH) (Feldman et al. 1998), and the water fraction of floor-bottom soils in some PSRs can reach 1700 ± 900 ppm hydrogen or 1.5 ± 0.8 wt.% water-equivalent hydrogen (Feldman et al. 2001). LEND neutron data (Mitrofanov et al. 2010, 2012) estimate that the polar regions contain a substantial fraction of water, up to 0.5 wt.% (weight percent) on average (Sanin et al. 2017).

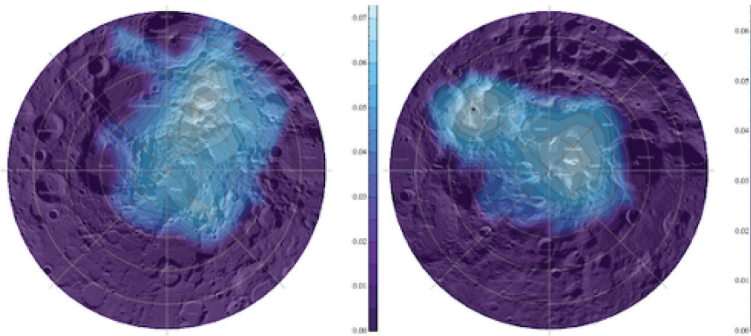

Figure 3. Lunar Prospector Neutron Spectrometer measurements of the epithermal neutrons are shown after conversion to abundance of water-equivalent hydrogen in the lunar north (**left**) and south (**right**) polar region. [Reproduced by permission of John Wiley & Sons from Miller RS, Nerurkar G, Lawrence DJ (2012) Enhanced hydrogen at the lunar poles: New insights from the detection of epithermal and fast neutron signatures. J Geophys Res 117:E11007 © 2012 American Geophysical Union,]

Other techniques are sensitive to the surface abundance of water, ice, or frost in the lunar PSRs. Lyman Alpha Mapping Project (LAMP) FUV albedo maps, probing tens of nm deep, indicate up to 2% water frost if intimately mixed with the lunar regolith (Gladstone et al. 2012) and 1–10% if ice is patchy but pure (Hayne et al. 2015). Unique IR absorptions of ice near 1.3, 1.5, and 2.0 μm were detected using the M^3 data near the lunar polar regions, and up to 30 wt.% surface exposed water ice was suggested (Li et al. 2018). Almost all M^3-derived ice locations also exhibited extreme LOLA reflectance (Fisher et al. 2017) and UV ratio values consistent with the presence of water ice, as well as annual maximum surface temperatures below 110 K (Li et al. 2018).

Albedo features on the floor of Shackleton Crater observed by LOLA were interpreted as a decrease in space weathering inside the crater, but could be consistent with surficial ice at abundances of 20% (Zuber et al. 2012). Japan's Kaguya lunar explorer also searched for lunar water ice. Using three dimensional reconstructed images inside the Shackleton Crater together with albedo data derived from Terrain Camera (TC) observations, Kaguya found exposed relatively pure water-ice deposits were not evident at the TC's spatial resolution; meaning that water ice either did not exist or was disseminated and mixed with soil at a few area percent

(Haruyama et al. 2008). Similarly, no bright regions consistent with exposed water ice were observed with LROC. Thomson et al. (2012) analyzed LRO Mini-RF images for Shackleton crater using a semi-empirical radar scattering model and found that an upper limit of about 5–10 wt. % water ice would be consistent with the observations.

When the LCROSS mission impacted into a PSR in Cabeus crater, it liberated water and other volatiles from the impact site into the exosphere where they were observed by the shepherding spacecraft, LRO, and Earth-based telescopes. Analysis of the NIR data from LCROSS yielded a detection of 155 ± 12 kg of H_2O in the field of view. Converting this to an estimated abundance yields 5.7 ± 2.9 wt.% water concentration in the Cabeus regolith (Colaprete et al. 2010). If extended to all PSRs (~30,000 km^2), this translates to ~2×10^{13} kg of water in the top meter of the regolith; however, neutron data are inconsistent with such prevalent water abundance. Other species like H_2S, NH_3, SO_2, C_2H_2 and CO_2 were also detected in the impact ejecta at abundance > 2% relative to water by mass (Colaprete et al. 2010; Table 1). LAMP observation of the LCROSS impact plume reveals 12 kg of Hg (Hurley et al. 2012a). These analyses considered potential contributions from the impactor and reported the volatiles that were derived from native lunar material. An important caveat to these abundance estimates is that assumptions must be made regarding the relationship between the amount of volatiles observed in the plume and the amount of host material from which it was derived. Hurley et al. (2012a) concluded that the volatility of the species vastly affected the amount that was released, with H_2 and CO being derived from the entire volume of the resulting impact crater, whereas the Hg was derived from the volume of material reaching sunlight. Thus, there are systematic uncertainties in LCROSS abundance estimates, both for absolute and relative abundance values, reported in the literature.

Table 1. Comparison of relative abundances of compounds derived from the LCROSS mission and from observations of comets. Note that the sublimation temperatures (T_{sub}) specified are for nebular conditions, and indicate relative rather than absolute volatility

	LCROSS abundance[a]			**Cometary abundance**
Compound	**Molecules/cm^2 [b]**	***X*/H_2O (%)**	**T_{sub}[c]**	***X*/H_2O (%) (Bockelée-Morvan et al. 2004)**
H_2O	$5.1 \pm 1.4 \times 10^{19}$	100	152	100
H_2S	$8.5 \pm 0.9 \times 10^{18}$	16.8	57	0.3–1.5
NH_3	$3.1 \pm 1.5 \times 10^{18}$	6	78	< 0.2–1.5
SO_2	$1.6 \pm 0.4 \times 10^{18}$	3.2	83	0.2
C_2H_4	$1.6 \pm 0.4 \times 10^{18}$	3.1	42	–
CO_2	$1.1 \pm 1.0 \times 10^{18}$	2.2	72	3.0–6
CH_3OH	$7.8 \pm 42 \times 10^{17}$	1.6	99	< 0.15–4
CH_4	$3.3 \pm 3.0 \times 10^{17}$	0.7	31	0.14–1.5
OH	$1.7 \pm 0.4 \times 10^{17}$	0.03	–	–
H_2CO	–	–	64	0.4–4
CO	–	–	25	< 0.4–30

***Notes*:**
[a]Colaprete et al. 2010;
[b]Note that the specified uncertainties in abundance are a combination of residual errors from a fit to LCROSS-NIR measurements, and uncertainties in the measurements themselves—for some species, the combined uncertainty is very large relative to the abundance derived by the fitting process;
[c] Sublimation temperatures from Yamamoto (1985).

2.1.2. Non-polar volatile abundances. Recent analyses of the relative abundance of H/OH as a function of soil maturity indicates that H/OH increases with maturity (Kramer et al. 2011), and maturity is related to exposure to solar wind (Sim et al. 2017). Early analyses of Apollo regolith samples place abundances of H in the 10–100 ppm range (DesMarais et al. 1974). These data provide an important benchmark for the calibration of remote sensing data.

Elemental hydrogen abundances have been evaluated for the non-polar highlands regions with Lunar Prospector epithermal neutrons counts (Fig. 4). In this context, hydrogen is interpreted to be implanted in the lunar regolith via solar wind bombardment. The mean elemental hydrogen concentration in the non-polar lunar highlands is 65 ppm (Lawrence et al. 2015). Highs between 120 to 165 ppm are observed in a variety of smaller, localized regions. Hydrogen depletions (<50 ppm) are often observed within the cavities of both craters and basins (e.g., Orientale). Most are younger (Eratosthenian and Copernican) and have hydrogen concentrations between 10–30 ppm, while some, despite being relatively old (Upper Imbrian to Pre-Nectarian), have hydrogen abundances between 30–50 ppm (Wilson et al. 2018).

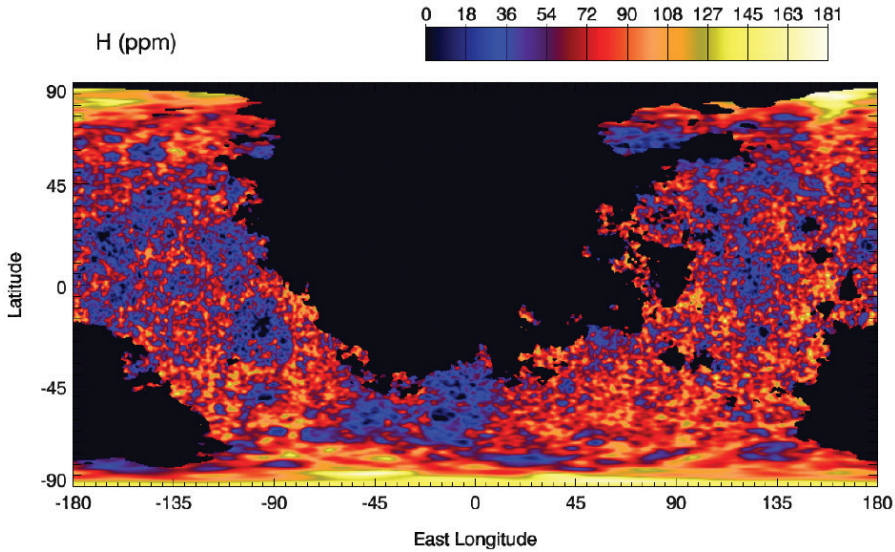

Figure 4. Distribution of the bulk H in the top several 10s of cm in lunar highlands is shown from neutron spectroscopy. [Reproduced from Lawrence DJ, Peplowski PN, Plescia JB, Greenhagen BT, Maurice S, Prettyman TH (2015) Bulk hydrogen abundances in the lunar highlands: Measurements from orbital neutron data., https://doi.org/10.1016/j.icarus.2015.01.005. Published by Elsevier Inc. Licenced under CC-BY-NC-ND 4.0]

Spectral reflectance measurements in the NIR from three different instruments on three different spacecraft, Cassini VIMS (Clark 2009), Chandrayaan-1 M^3 (Pieters et al. 2009), and EPOXI High Resolution Instrument-infrared spectrometer (HRI-IR), (Sunshine et al. 2009), showed that a surface layer of OH and water exists globally and varies across the surface as a function of the solar phase angle. Water abundance increases as a function of latitude, from less than 100 ppm to ~750 ppm to poles (Li and Milliken 2017). The H/OH content may reach ~1000 ppm at the polar regions (Clark 2009). These measurements are restricted to the surface of the Moon. To convert to an absolute quantity, one must assume a depth for the hydration layer. This is an area of ongoing investigation. Furthermore, abundance estimates based on NIR measurements are highly dependent on accurate models of the contributions to the reflectance spectra due to photometry and thermal emission (e.g., Clark 2009; Bandfield et al. 2018).

LRO LAMP data measure hydration via diurnal variation in spectral slope in the 164–173 nm range, where H_2O absorbs strongly (Hendrix et al. 2012, 2019). Slopes are redder (consistent with more hydration) later in the day and at higher latitudes and bluer (consistent with a loss of hydration) within ~two hours of local noon. Maximum abundances are estimated at 1% by volume. Like the NIR observations, these are surficial measurements.

2.2. Composition

2.2.1. Permanently shadowed regions. Spectroscopy within the PSRs is difficult because there is no direct illumination source for which to provide spectra. The most complete peek into the composition of volatiles in the lunar PSRs came from the LCROSS impact, where material was lofted into sunlight and spectra could be obtained. Remote sensing of the vapor plume released during the impact from LRO revealed H_2 and CO in the plume (Gladstone et al. 2010). However, these molecules are not thought to be stable against sublimation at the temperatures in PSRs. It is unknown whether those compounds exist in the PSRs or if they were synthesized during the impact (Hurley et al. 2012a). LAMP also saw a signal at 185 nm that can be attributed to a combination of Hg, Mg, and Ca. The presence of Hg in the polar regions was predicted by Reed (1999), based on Hg concentrations in Apollo drill cores thought to be derived from a comet impact. The NIR spectra from LCROSS are comprised primarily of H_2O; with additional constituents of H_2S, NH_3, SO_2, C_2H_4, CO_2, CH_3OH, CH_4, OH also inferred. From a telescope on Earth, Killen et al. (2010) observed Na in the plume.

Within the PSRs spectroscopy relies on either active illumination sources, e.g., LOLA, or singly or doubly reflected light from illuminated walls and peaks. LRO/LAMP uses starlight as the illumination source to gather FUV reflectance spectra from within the PSRs. The off/on albedo measured by LAMP is consistent with the presence of water ice in some PSRs (Gladstone et al. 2012; Hendrix et al. 2012; Hayne et al. 2015). Correlation of enhanced reflectance (LOLA) in PSRs with low surface temperatures suggest possible CO_2 and H_2O sequestration at surface (Fisher et al. 2017).

The presence of Ar in PSRs is hypothesized from the distribution of Ar in the Moon's exosphere (Grava et al. 2015; Hodges 2018). Argon also adsorbs to the lunar nightside, showing that the interaction between Ar and the regolith enables trapping of Ar at temperatures above its nominal stability temperature (Zhang and Paige 2009). This emphasizes the complex nature of the interaction between volatiles and the lunar regolith. Thus, the presence of H_2 and CO in the LCROSS plume may reveal an enhanced ability of lunar regolith to trap these species beyond the nominal sublimation description of the stability shown in Figure 2 (Farrell et al. 2017).

2.2.2. Non-Polar. The primary distinction for volatiles outside of the polar regions is whether the observed hydration is OH or H_2O. Absorptions due to OH vibrations commonly occur at wavelengths of ~2.65–2.9 μm, whereas fundamental stretching vibrations of H_2O occur near ~2.9 μm and the first overtone of the H_2O bending vibration occurs near ~3.1 μm. However, the position and strength of OH absorptions are highly variable and can occur at wavelengths >2.9 μm depending on bonding energy and the cation to which hydroxyl is attached. Thus, OH absorptions may be broad and occur throughout the ~2.65–3.5 μm range (Beran and Rossman 2006). At much coarser global scale, measurements of the Moon made by HRI-IR on EPOXI, which collected high spectral-resolution data to beyond 4 μm, shows a maximum absorption near 2.8 μm, more consistent with OH than H_2O as the dominant molecular species (Sunshine et al. 2009) (Fig. 5). The wavelength range of M^3 ends at 2.976 μm, meaning that the full shape and wavelengths of maximum absorption that would distinguish OH from H_2O are not measured by M^3.

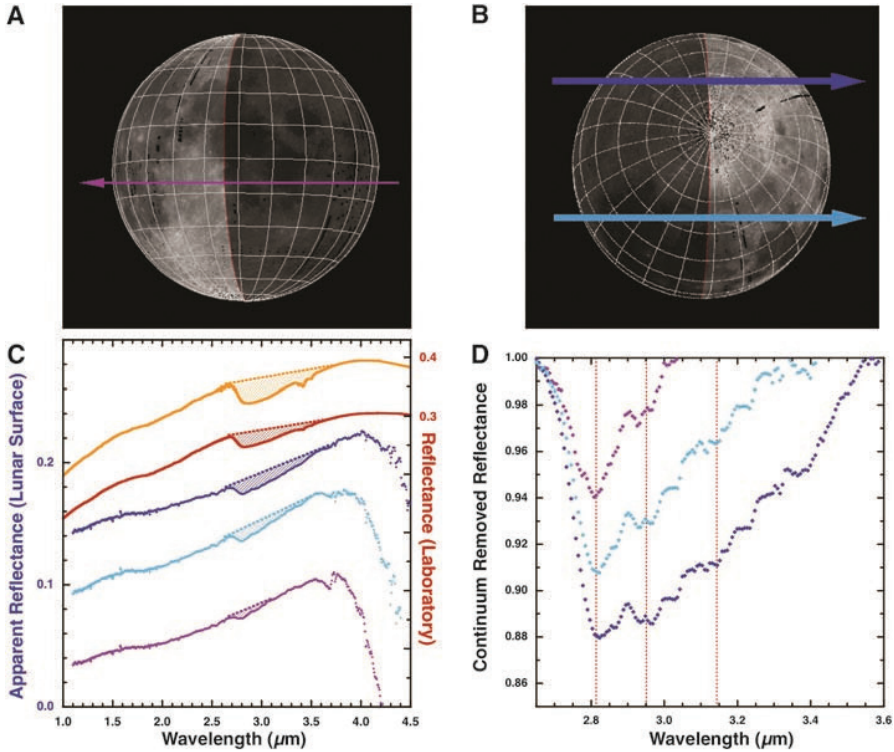

Figure 5. Reflectance spectra from three chords (**purple, blue, cyan**) are shown compared to laboratory spectra of lunar soils (**orange and red**) demonstrate the OH/H_2O absorption features at 2.8, 2.95, and 3.14 μm. [From Sunshine JM, Farnham TL, Feaga LM, Groussin O, Merlin F, Milliken RE, A'Hearn MF (2009) Temporal and spatial variability of lunar hydration as observed by the Deep Impact spacecraft. Science 326:565–568. Reprinted with permission from AAAS.]

2.3. Distribution

2.3.1. Permanently shadowed regions. The apparent distribution of volatiles in PSRs is heterogeneous on many spatial scales, from ~100 m up to 100's km, suggesting heterogeneity in both the lateral distribution and the depth distribution. Comparing one PSR to another reveals that they do not have the same apparent volatile content, which is somewhat surprising if the source of volatiles is a uniform input from external sources. Closely co-located PSRs with similarly old, cold and dark interiors have surprisingly variable evidence for surface frost and hydrogen (i.e., water) contents. In fact, different datasets related to surface frost also do not completely agree with one another.

Both LAMP and LOLA show non-uniform albedo in all cold traps, which indicates a heterogeneous distribution of water ice exposed on the surface (Gladstone et al. 2012; Lucey et al. 2014; Hayne et al. 2015; Fisher et al. 2017), as shown in Figure 6. Within an individual PSR, the water distributions are also heterogeneous. For example, both LOLA and LEND data indicate enhanced hydration in the poleward facing slopes than equator facing slopes (Lucey et al. 2014; McClanahan et al. 2015). Evidence for surface ice (Gladstone et al. 2012; Lucey et al. 2014; Hayne et al. 2015) appears to be especially abundant in locations with surface temperatures <110 K (Fisher et al. 2017), which may be related to the preference for pole-facing slopes. Additionally, spectral mapping using M^3 data provides a third corroborating data set for the heterogeneous distribution of exposed water frost in lunar PSRs (Li et al. 2018).

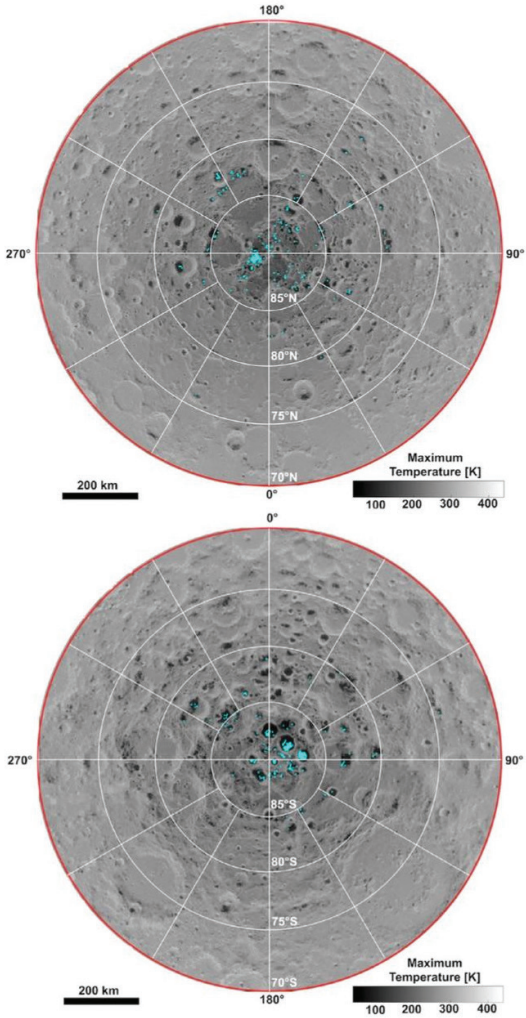

Figure 6. The maps of the North Pole **(top)** and South Pole **(bottom)** of the Moon depict the maximum temperature of each pixel from LRO Diviner in **grayscale**. The **cyan points** indicate where anomalous brightness is observed with the LRO LOLA laser reflectance. [Reproduced from Fisher et al. (2017)]

Understanding of the depth distribution is enabled by comparing remote sensing techniques that are sensitive to different depths. Whereas the NIR and FUV measurements are only sensitive to the top few microns at the surface, neutron data reflect bulk hydrogen integrated over a 1 m depth. If the "frost" features shown in Gladstone et al. 2012 were actually to indicate 1–2 wt.% H_2O throughout the top 1 meter of regolith, the neutron flux effects measured from orbit would be much larger than are observed. So the "frost" features must be limited in depth extent. LEND data have been interpreted in terms of a uniformly distributed concentration of 0.3–0.5 wt.% WEH in PSRs. But fast neutron measurements from Lunar Prospector suggest top 10–20 cm of polar regions is relatively dry compared to deeper levels (Feldman et al. 1998, 2000, 2001). An exception is Shackleton crater, where LPNS fast neutron data shows evidence for surface/shallow hydrogen/ice with 0.7 wt.% water-equivalent hydrogen (Miller et al. 2014). A thin layer of frost would not affect the fast neutrons, so if the FUV and NIR signatures are of H_2O frost, it is a surficial layer and not homogeneously distributed with depth. Subsurface abundances could be higher than the average 0.3–0.5 wt. % if the overburden is drier (Sanin et al. 2017).

Interestingly, the epithermal neutron flux is affected by surface frost (Lawrence et al. 2011). A surface frost can enhance the thermal neutron flux. The high-energy tail of this enhancement begins to fill in the deficit of epithermal neutrons caused by hydrogen at depth. Thus, the disparity between the observation of surface frost in Haworth from LAMP and the lack of neutron signature there may be explained by this interference effect.

The LCROSS impact excavated material from 2–3 m depth. Material in the plume probed the deepest into a PSR of any present data set. While the impact targeted a location with a known large hydrogen signature, the abundance of water in the plume was higher than inferred from the neutron data (Colaprete et al. 2010). The amount of enrichment that stemmed from the excavation below the nominal 1 m extent of the neutron measurements vs. from a "lucky strike" in a localized enriched region compared to the average in the larger footprint of the neutron

measurements remains ambiguous and cannot be resolved with the existing data. However, Mini-RF monostatic observations, which are capable of detecting blocky ice deposits within a few m of the surface, did not find them at the LCROSS impact site (Neish et al. 2011).

2.3.2. Non-polar. The distribution of OH/H_2O globally is presently debated. Initial interpretation of M^3 and EPOXI data showed a latitudinal and local time distribution of the OH/H_2O signature in the NIR data (Pieters et al. 2009; Sunshine et al. 2009; McCord et al. 2011). Both morning and afternoon data exhibit increased absorption strengths compared with spectra acquired near local noon, particularly for latitudes equatorward of 60°N/S. At higher latitude there is no clear diurnal variation of lunar surface water, i.e., the water appears to persist (Pieters et al. 2009; McCord et al. 2011). The maximum diurnal variation of lunar surface water could reach 200 ppm assuming 60–80 μm particle size (Li and Milliken 2017). Analysis and improvements to the M^3 data is ongoing work because accurate determination of the global OH/H_2O distribution and abundance is contingent on the data reduction methods used to account for the effects of thermal emission (Li and Milliken 2016; Woehler et al. 2017; Bandfield et al. 2018) and phase function (Clark 2009) on spectral data.

A latitudinal and local time variation in the global surface hydration is supported by LAMP FUV data (Hendrix et al. 2019). Measurements at FUV wavelengths detect a diurnal variation in the photometrically-corrected spectral slope around the H_2O absorption edge near 165 nm (Hendrix and Hansen 2008) on the dayside of the Moon (Hendrix et al. 2012). The spectral slopes are reddest (consistent with greater levels of hydration) early and later in the day; the slopes become bluer approaching local noon, consistent with a loss of hydration due to thermal desorption (see Fig. 7). The hydration signature is stronger and has more variability in the highlands than in the mare. Abundances measured in these observations, which sense only the top layer of grains of the regolith, is on the order of a monolayer.

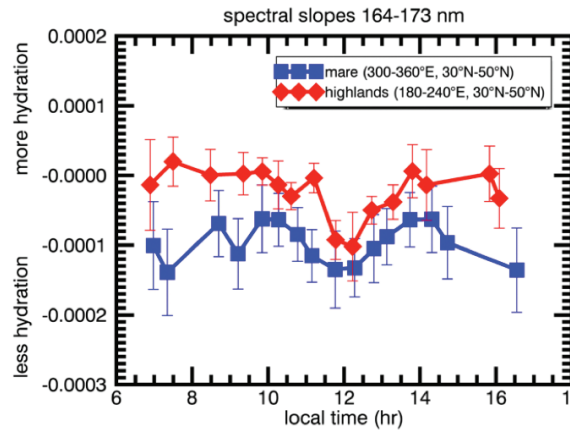

Figure 7. FUV spectra indicate a local time and latitude dependence consistent with a depletion of surface hydration at low latitudes and near noon. Mare regions exhibit less hydration than highlands. [Reproduced from Hendrix et al. (2019)]

Meanwhile, further corroborating evidence has remained elusive. For example, LRO observations from CRaTER and LEND have been interpreted to contain local time (Livengood et al. 2015; Schwadron et al. 2018) variations. However, the magnitude of the diurnal effect suggested by the LEND data is great enough that it should also have been observed by other means (Starukhina 2012). The CRaTER observation of knock-on protons enhancement at the

terminator could support this, but there are relatively few data points. Consequently, the CRaTER instrument is collecting observations of these knock-on collisions at more locations and local times of day. With these data, it may be possible to resolve this debate (Schwadron et al. 2018).

2.3.3. Seasonal variability. Another factor in temporal variability is the possible presence of seasonal cold-traps. LADEE NMS measured long-term variations of lunar exospheric argon (Hodges and Mahaffy 2016). Figure 2 of that paper shows that the "argon anomaly" (the deviation from a mission-average profile) can be approximated by a semiannual sinusoid, with peak around January. Models demonstrate that cold traps form at the lunar poles at the respective winter, and release volatiles back again with the equinox (Grava et al. 2015). Interestingly, the January peak occurs one month after the Moon's vernal equinox (December), suggesting that there is a time lag in the release of polar volatiles which may be related to thermal inertia effects and to lateral transport in the exosphere.

2.4. Physical form

2.4.1. Polar regions. After Clementine, there was considerable debate regarding whether coherent ice blocks exist on the Moon (Nozette et al.1996; Simpson and Tyler 1999). Nozette et al. (1996) found an enhanced circular polarization ratio (CPR) at zero-phase angle over Shackleton crater, which is located at the south pole and contains PSR. However, no discernible CPR enhancement was observed for nearby craters that are in sunlit regions. The enhanced radar signal from Shackleton crater is explained as probable evidence of large quantities of water ice (Nozette et al. 1996). However, a later reanalysis of the same data set using a different processing technique by Simpson and Tyler (1999) indicated that the enhanced CPR could also result from surface roughness or blockiness, which does not require the presence of water ice.

At the same time, Earth-based radar with high spatial resolution was used to search for the presence of ice deposits. However, the observations show negative results (Stacy et al. 1997; Campbell et al. 2006), leading to the conclusion of no thick, coherent water ice deposits over the lunar polar regions. Their ~70 cm wavelength observations should penetrate several to tens of meters in depth depending on the angle of the observation and the material properties. This currently stands as a limit on the depth to which radar-coherent ice exists on the Moon.

To resolve the previous controversy on radar detection of water ice deposits, two orbital miniature synthetic aperture radars (Mini-SAR and Mini-RF) on the Chandrayaan-1 and Lunar Reconnaissance Orbiter (LRO) missions have imaged the lunar surface since 2008. However, the presence of coherent, thick, pure ice in the PSRs remains controversial. Spudis et al. (2010, 2013) analyzed Mini-SAR and Mini-RF images and found some craters within PSRs with elevated CPR in their interior regions, but not external to their rims, which is different from those of fresh craters. Based on the CPR characteristics, the locations and the correlations with Lunar Prospector (LP) neutron data and thermal conditions, these radar anomalous craters were interpreted as potential sites for water ice deposits. If high-CPR deposits in anomalous craters contains water ice, then there could be about 600 million metric tons of water ice in total over the north polar region based on a rough estimation. However, further analyses of these anomalous craters offered alternative explanations for the anomalous polar craters (Fa and Cai 2013; Eke et al. 2014; Fa and Eke 2018). They found that polar anomalous craters are not over abundant, are consistent with surface and subsurface rocks, and likely represent an intermediate stage of normal crater evolution instead of evidence of water ice.

From 2012 to 2015, Mini-RF also conducted bistatic radar observations together with Arecibo radar, and imaged a variety of terrains over the lunar nearside, including mare, highland, pyroclastic, and crater ejecta and floor. Patterson et al. (2017) found that radar signals from a sunlit region of the floor of Cabeus crater are unique with respect to other terrains, and further analysis suggests this unique response may indicate the presence of water ice deposits at depth (see Fig. 8).

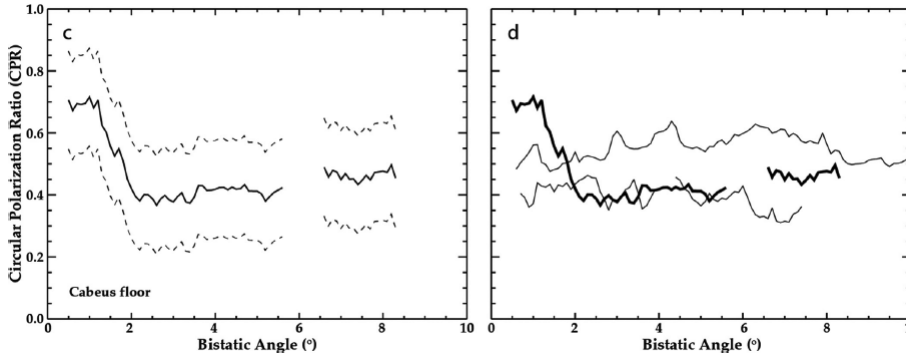

Figure 8. Mean CPR (**solid line**) and its uncertainty (**dashed lines**) as a function of bi-static angle are shown for a region on Cabeus floor (**left**). The right-hand plot compares the Cabeus mean CPR (**black line**) with CPR of typical highland materials and radar facing slopes (**gray lines**). Bistatic radar response at low bistatic angles reveal an enhanced CPR ratio in Cabeus crater compared to similar terrains, consistent with ice. [Reproduced from Patterson et al. (2017)]

However, Neish et al. (2011) compared monostatic data from the pre- and post- LCROSS impact Mini-RF images of the PSR portion of Cabeus crater. CPR for the crater floor of Cabeus was comparable to or less than the average of nearby terrain, suggesting no presence of thick deposits of nearly pure water ice within a few meters of the lunar surface even where LCROSS revealed the presence of water ice. Ice deposits smaller than decameter blocks could be consistent with the data.

LCROSS data combined with numerical modeling suggests that the water ice within Cabeus Crater is commingled with lunar regolith. Water ice particles within the impact ejecta cloud simultaneously photo-dissociated and sublimated after reaching sunlight (Colaprete et al. 2010; Heldmann et al. 2015). An analysis of the UV–visible spectral data suggests that the dust particles ejected into the impact plume were likely submicron to micron in size (Heldmann et al. 2015). Post-impact, the UV–visible spectrum of the impact plume demonstrated significant changes in color which are indicative of the scattering properties in the plume. Post-impact, the spectra became bluer, indicating a decrease in scattering particle size most likely due to ice grain sublimation and the break-up of loosely consolidated grains held together by volatiles. An increase in OH was also observed and attributed to the photodissociation of water ice in sunlight. These observations, combined with the detection of water ice bands in the near-infrared, indicate the presence of water ice and vapor in the impact plume. The trends in the spectral data suggest the impact plume contained populations of both pure water ice grains as well as dirty ice grains (e.g., aggregates of regolith and ice) (Heldmann et al. 2015).

Additionally, the form of the IR water absorption line can reveal information about the form of water ice. The 1.5 μm absorption of M^3 spectra of ice-bearing pixels in PSRs shifts 0.05 μm toward the longer wavelengths, suggesting low-density ice condensed from vapor phase that might be associated with impacts and water migrations through the lunar exosphere (Li et al. 2018). However, this interpretation is not unique and is based on data with low signal-to-noise ratio.

2.4.2. Non-polar regions. The M^3 signatures of water are likely dominated by two components. The first is the bulk OH content of agglutinitic glass (Liu et al. 2012, see Fig. 9), which may be stable over diurnal cycles and contains a solar wind component trapped/quenched during formation. The second is OH in grain rims that is potentially dynamic over diurnal cycles due to ongoing regolith–solar wind interactions (e.g., Farrell et al. 2017). Both OH and H_2O are expected products of the reduction of ferrous iron to nanophase iron (Housley et al. 1973); meanwhile, solar wind H implantation can form trapped OH in grain rims, a

portion of which is expected to react to form H_2O at elevated temperatures (e.g., Jones et al. 2018). The distinction between OH and H_2O is, however, unclear from current spectral observations. With increased exposure to the space environment the abundance of agglutinates and glassy rims on soil grains increases, as does the abundance of nanophase iron.

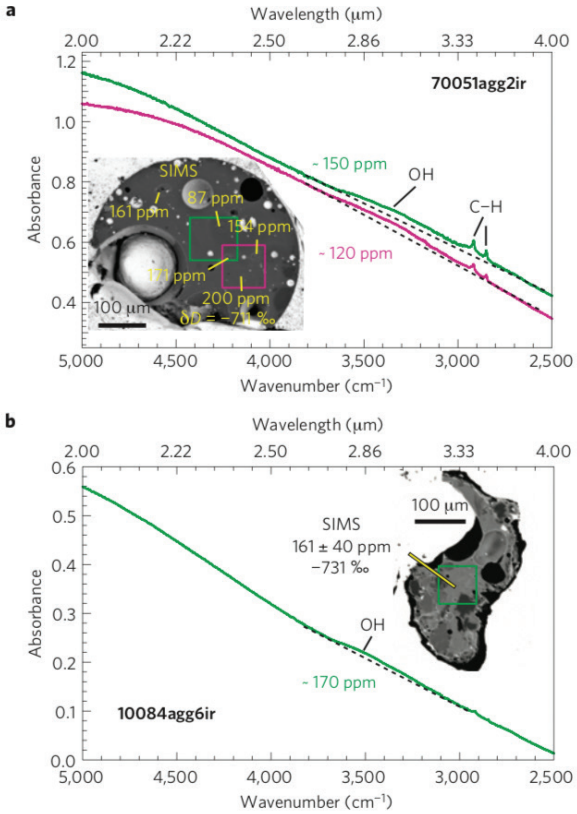

Figure 9. Analysis of lunar agglutinates shows OH at levels of >100 ppm in the glass. [Reproduced by permission of Springer Nature © 2012 Liu Y, Guan Y, Zhang Y, Rossman GR, Eiler JM, Taylor LA (2012) Direct measurement of hydroxyl in the lunar regolith and the origin of lunar surface water. Nat Geosci 5:779–782.].

3. VOLATILE SYSTEM

Next, we examine the various processes associated with lunar volatiles. These factors include sources of volatiles, mechanisms modulating the distribution of volatiles, and sinks of volatiles. Determining the relative importance of these processes is ongoing work. All of the processes described in this section and their interactions with one another contribute in some regard to lunar volatiles.

3.1. Impacts

3.1.1. Comets. Several observational datasets suggest that asteroid and comet impacts may have contributed to the lunar polar volatile inventory (e.g., Arnold 1979; Colaprete et al. 2010; Miller et al. 2014). Carbonaceous chondrite-like asteroids with properties resembling CM and CI meteorites may have >10% water (by mass) in the form of hydrated silicates, while comets are ice-rich and some asteroids may be ice-rich. Recent dynamical work using the

model of Granvik et al. (2016, 2017) indicates that most lunar impactors are asteroids (Bruck Syal and Schultz 2014). Analysis of the isotopic compositions of lunar samples also suggests that asteroids were the dominant source of lunar water, with comets contributing to a lesser degree—at least during the initial ~200 Ma of the Moon's history (Barnes et al. 2016).

Comets and asteroids with masses greater than 10^{12} kg are estimated to impact the Moon with frequencies of ~1×10^{-7} yr^{-1} (Ong et al. 2010; Bruck Syal and Schultz 2014). Based on hydrocode simulations of volatile retention for a range of impact velocities, and approximate rates of volatile transport and survival, Ong et al. (2010) estimate that 1.3×10^{11}–4.3×10^{12} kg of cometary water and 2.7×10^{13} kg of water from hydrated asteroids could survive in lunar cold traps over 1 Ga. Stewart et al. (2011) model post-impact volatile transport in more detail (for a single impact scenario) and extrapolate their results to estimate that the polar cold traps may contain 5.0×10^{10}–1.6×10^{11} kg of cometary water. However, these estimates may be affected by factors such as the influence of impact angle on the retention of impactor material (Pierazzo and Melosh 2000; Artemieva and Shuvalov 2008) and the extent to which water can be liberated from hydrated minerals (Svetsov and Shuvalov 2015).

Although most of the work discussed above has focused on water, impactors can deliver multiple volatile species to the lunar surface; the composition of cold-trapped volatiles may be influenced by photochemistry and chemical reactions in an impact-generated atmosphere (Berezhnoy 2013). The transformation of the lunar exosphere into a collisional and/or optically thick atmosphere after a volatile-rich impact may also affect the contribution of such impacts to the lunar volatile inventory—factors such as atmospheric self-shielding from photodestruction, diversion of the solar wind, and gas dynamic interactions between multiple species may act to enhance or impede the cold-trapping of impact-delivered volatiles (Prem et al. 2015).

3.1.2. Meteoroids. Meteoroids are continually bombarding the surface of the Moon, delivering exogenous material to the lunar environment. Most meteoroids are thought to have a composition similar to carbonaceous chondrites (Anders 1964), which would comprise a source of hydrogen and carbon bearing materials. Sporadic meteoroid impacts occur all over the Moon; however, the flux is not isotropic. Szalay and Horányi (2015) demonstrate from LADEE Lunar Dust Experiment (LDEX) data a peak flux near the dawn terminator of the Moon owing to the motion of the Earth–Moon system revolving around the Sun. Lesser peaks near 11 am and 1 am local times derive from populations moving away and towards the Sun, respectively. The Earth–Moon system encounters meteor streams of dust leftover from passing comets. These meteor streams result in higher impact rates for a few days.

Meteoroid impact velocities are >10 km/s, which is high enough to cause melting and vaporization of parts of the impactor and the target lunar material. Thus, water can be liberated during the impact from hydrated material in the impactor or adsorbed OH/H_2O on the Moon. However, the temperature of the vapor plume is expected to be ~5000 K, which is high enough that a significant fraction of liberated water would escape from the Moon. Assuming ~⅓ of the water remains, this is still a significant source of water to the lunar inventory.

The LADEE NMS detected water or OH in the lunar exosphere. LADEE was constrained to low latitudes, so no data were acquired at high latitudes. LADEE's detections of exospheric water or OH were stochastic and have no clear relationship to altitude or local time of the measurement. However, the observed density is generally higher during meteor streams. Further, analysis of the occurrence rate of density is reproduced using a model of water or OH released by meteoroid impacts (Benna et al. 2019).

3.2. Impact gardening

Where sublimation-driven transport is negligible, the primary driver of the depth and lateral distribution of volatiles in the regolith is impact gardening (e.g., Gault et al. 1974;

Morris 1978). Meteoroids act to mix or "garden" the lunar soil, removing regolith material from depth to redeposit it near the surface in an ejecta blanket or bury and insulate proximal regolith from further space weathering under an ejecta blanket (see Fig. 10). While impact bombardment acts to both expose and obliterate buried volatiles and sequester and shield them, the effects of meteoroid bombardment are primarily protective. An impact distributes ejecta much further laterally than it excavates vertically and any given point on the lunar surface is likely to be buried more times than excavated (Arnold 1975; Crider and Vondrak 2003). However, for impacts into PSRs, the icy ejecta can be removed from the PSR and distributed on the surface outside of the PSR. Farrell et al. (2013) proposed this as a mechanism to supply the surface hydration at high latitudes observed in the IR and FUV.

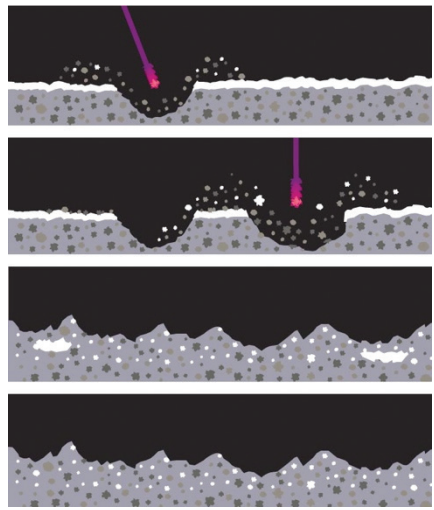

Figure 10. A depiction of impact gardening demonstrates the protective nature of an ejecta blanket, burying a layer of reworked regolith deep enough that it reduces the likelihood that later impacts reach it. After Vondrak and Crider (2003).

While the effects of impacts are primarily protective, most vapor-producing gardening occurs in the topmost layer of soil under torment of the high flux of micrometeoroids (Gault et al. 1974; Arnold 1975). Micrometeoroid impacts are frequent and have very small lateral extent, producing poor protective ejecta. Most authors studying micrometeoroid impact vapor production have relied on studies of micrometeoroid impact effects (Gault et al. 1974; Hartung and Storzer 1974; Hörz 1975) and a vapor production model from Cintala (1992). Recent results from LADEE (Horányi et al. 2015; Szalay and Horányi 2015) have greatly increased our understanding of micrometeoroid flux and the rate of surface gardening. Future work will benefit from these results as we continue to explore the role that impact bombardment plays in the survival of surface volatiles.

3.3. Charged particle irradiation

3.3.1. Solar wind. The solar wind is a flow of ions, primarily protons and electrons, at speeds of ~400 $km \cdot s^{-1}$ radially outward from the Sun. Because the Moon has neither a substantial global magnetic field nor thick atmosphere to divert the flow, these ions come into direct contact with the surface of the Moon. As such, the solar wind represents a nearly constant supply of the building blocks of volatiles, including H, He, C, N, and O. Most incident ions penetrate up to 10 nm into the grain of regolith they encounter, neutralize, and become implanted. The Moon's monthly passage through the Earth's magnetotail offers a method for

separating out the solar wind's role in volatile processes compared to other processes. Any prompt response of the Moon to the solar wind should exhibit temporal variability owing to the 5 days in which the ion flux to the Moon is reduced.

In addition to theoretical work (Starukhina 2001, 2006; Farrell et al. 2015; Tucker et al. 2019), significant progress has been made in measuring the reaction pathways of solar wind protons in their interaction with the lunar regolith (see Fig. 11). MAP-PACE onboard Kaguya has detected protons backscattered from the surface of the Moon in the amount of 0.1–1% of the incident flux (Saito et al. 2008). Energetic neutral atom imagers on both IBEX and Chandrayaan-1 detected hydrogen atoms that are backscattered off of the surface at energies close to the incident proton energy indicating that 10–20% of incident protons interact weakly with the surface; only picking up an electron and exchanging little energy (Wieser et al. 2009). Hodges (2011) predicts that a large fraction of the remaining proton flux is neutralized and thermalized and released as neutral hydrogen. To date, this atomic hydrogen corona has not been observed on the Moon, although it has on Mercury (Broadfoot et al. 1976; McClintock et al. 2008). However, LRO LAMP has detected a molecular hydrogen exosphere of the Moon (Stern et al. 2013) that accounts for 10–50% of the incident solar wind flux (Hurley et al. 2017). The LADEE NMS instrument measured CH_4 in the lunar exosphere (Hodges 2016) that could account for 0.01% of incident protons. There remains the possibility that significant amounts of the solar wind protons are implanted and remains available for conversion to OH and/or H_2O.

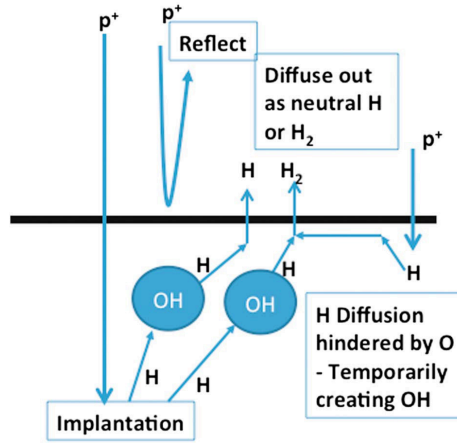

Figure 11. Interaction pathways for implanted solar wind hydrogen are shown. [Reproduced from Farrell et al. (2017).]

Originally postulated by Zeller et al. (1966), solar wind hydrogen can interact with oxygen in the lunar regolith to form OH (Starukhina 2001) and possibly H_2O (Dyar et al. 2010). Solar wind hydrogen is a potential source of the latitudinally and diurnally varying OH/H_2O observed by Cassini VIMS (Clark 2009), EPOXI (Sunshine et al. 2009), and M^3 (Pieters et al. 2009; McCord et al. 2011). Experimental measurements simulating solar wind bombardment of lunar analog silicates (amorphous SiO_2 and olivine) have shown that the increase in the OH signal at ~3 μm is sufficient to explain the lunar noon absorption signal at the lunar equator (Ichimura et al. 2012; Schaible and Baragiola 2014). However, not all laboratory experiments produce the same results (Burke et al. 2011; Managadze et al. 2011; Meyer et al. 2011). Further, Izawa et al. (2014) analyzed Apollo samples in a carefully controlled environment and found the presence of the 3 μm absorption without irradiating the sample in the lab. This was interpreted to mean that hydration was bound within the sample. Heating of hydroxylated

lunar soils to greater than ~500 K can lead to dissociative recombination of hydroxyl and formation of molecular water (Poston et al. 2015). Although the lunar surface never reaches this temperature, it is possible, transiently, during meteorite impacts.

Species on the surface of exposed regolith can be removed from lunar grains by incident solar wind ions in a process known as sputtering. The sputtering cross-section of sub-monolayer water deposited on loose lunar regolith grains has been measured in the laboratory (Mitchell et al. 2013). The yield is less than one, meaning that there is a net deposition of solar wind protons through the ion bombardment. However, sputtering yields on ices exceed one, and therefore are a net loss of water can occur due to sputtering in PSRs (Johnson 1989; Johnson and Baragiola 1991; Lanzerotti et al. 1981). Zimmerman et al. (2012) simulate the access of solar wind ions to a polar crater and find that asymmetric sputtering is expected with the highest input fluxes to the equatorward facing crater wall. Sputtered water molecules are relatively energetic and have a chance of escaping lunar gravity (Crider and Vondrak 2002). Those particles that do not escape can be deposited outside of the PSRs (Farrell et al. 2013).

3.3.2. Energetic particles. In PSRs, even buried water ice can undergo radiolysis driven by energetic charged particles accelerated outside the heliosphere and in solar flares and coronal mass ejections. For overviews of the radiolysis of ices on Mercury and water ice in the outer Solar System, see Delitsky et al. (2017) and Johnson (2011), respectively. Solar energetic particles (SEPs) can penetrate the regolith to depths of ~1 mm, while galactic cosmic rays (GCRs), can penetrate tens of centimeters (Jordan et al. 2013). SEP ions cover an energy range of ~50 keV/nucleon to 10 GeV/nucleon, and the electrons range from ~1 keV to ~10 MeV. Both ions and electrons, however, have fluxes that peak at energies lower than this range (McGuire and von Rosenvinge 1984). GCRs, on the other hand, have much lower fluxes but much higher energies: GCR protons, which account for >80% of all GCRs, have a peak flux near 200 MeV (Smart and Shea 1985). Because of their large gyroradii, both GCRs and SEPs are nearly isotropic at the lunar surface, even at locations not directly exposed to the Sun.

GCRs and SEPs deposit energy in the lunar regolith at a rate measured by the Cosmic Ray Telescope for the Effects of Radiation (CRaTER) on the Lunar Reconnaissance Orbiter (LRO). GCRs deposit about 0.022 eV/(molecule·Myr) (Schwadron et al. 2012), and SEPs about 0.24 eV/(molecule·Myr) (Jordan et al. 2013). Over time, the regolith is mixed by meteoroid impacts, exposing new material to these particles.

GCRs and SEPs can dissociate the water molecules in PSRs and create secondary products (e.g., Johnson 2011). One product is H_2, which LAMP on LRO detected unexpectedly in the impact plume created by the LCROSS mission (Gladstone et al. 2010; Hurley et al. 2012a). GCRs and SEPs may, on timescales of ~10^9 yr, drive enough radiolysis to create a significant fraction of the H_2 in the plume (10–100%). Consequently, energetic charged particles can drive losses of volatiles, by dissociating water, but can also create other volatiles, like H_2. They can energize the conversion of local material into organic compounds if the proper feedstock exists (Crites et al. 2013).

3.4. Outgassing

Anomalously high-OH contents observed with M^3 data at lunar pyroclastic deposits and silicic domes may indicate outgassed water from the lunar interior (Milliken and Li 2017). Needham and Kring (2017) discussed the vast contributions of the mare forming events to the lunar volatile inventory early in the Moon's history (see Fig. 12). The high rate of mass addition to the exosphere could lead to a long-lived, collisional atmosphere on the Moon (Vondrak 1974).

Alpha-particle spectrometers onboard of Apollo 15 and 16 measured anomalously high emissions of ^{222}Rn (Gorenstein and Bjorkholm 1973) and ^{210}Po (Gorenstein et al. 1974), a daughter of ^{222}Rn. Because of their short half-life (3.8 days), these measurements provided the tantalizing hypothesis that radioactive gases are leaking out of the lunar surface into the

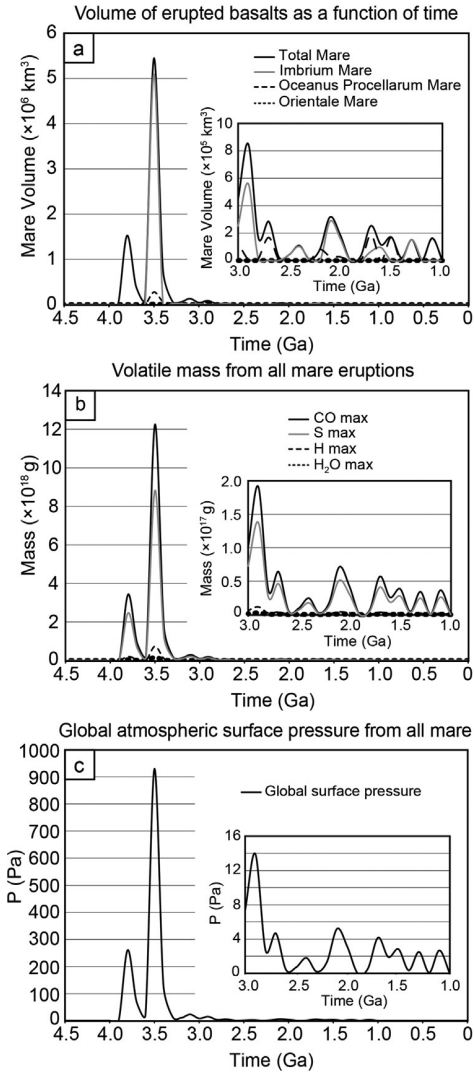

Figure 12. Timing estimates of the mare formation events are used to model the volatile addition rate and evolution of a global atmosphere over time. [Reproduced from Needham and Kring (2017), https://doi.org/10.1016/j.epsl.2017.09.002.]. Published by Elsevier BV. Licenced under CC-BY-NC-ND 4.0

exosphere (Crotts 2008). Interestingly, the Lunar Prospector Alpha Particle Spectrometer confirmed an enhancement of ^{222}Rn close to the Aristarchus plateau (Lawson et al. 2005). The locations where most events occur are the edges of the lunar maria, and in particular Aristarchus and Grimaldi. It is possible that these emissions are associated with leakage of other volatiles as well. In fact, the mass spectrometer LACE deployed on the lunar surface during the Apollo 17 mission at the edge of Mare Serenitatis and Mare Tranquillitatis, measured ^{40}Ar (besides He). Argon-40 is a radiogenic product of ^{40}K, and LACE detected variations in exospheric densities that have been hypothesized to correlate with shallow moonquakes measured by the four seismometers deployed on the lunar surface during the Apollo 12, 14, 15, and 16 missions (Hodges 1977). The role of such moonquakes would be to open up pores and cracks where gases released from the interior are trapped.

Likewise, helium in the lunar exosphere may be in part derived from leakage from the lunar interior. Although it is well-established that the majority of helium comes from solar wind alpha particles that become neutralized on interaction with the lunar surface (Hodges and Hoffman 1974; Feldman et al. 2012), correlating the upstream alpha particle flux measured with ARTEMIS with LAMP and NMS data provides an estimate that ~20% of the lunar helium is temporally decoupled from the upstream alpha flux (Benna et al. 2015; Hurley et al. 2016). This could be helium outgassing from the lunar interior or solar wind helium that resides in the regolith for long times.

Lastly, the recent LADEE equatorial orbiter carried a Neutral Mass Spectrometer (NMS) which detected ^{40}Ar in the lunar exosphere (Benna et al. 2015). Interestingly, the density was enhanced above the Western maria, which is rich in KREEP deposits. So, argon (and other volatiles) may be outgassing from that region, although the alternative explanation of a higher heat absorption, and hence a stronger interaction with the lunar surface, has been proposed (Hodges and Mahaffy 2016). Why these outgassing events happen at the edge of maria is not clear yet Crotts (2008) provides a review of this topic.

3.5. Thermal processes

3.5.1. Thermal mapping, illumination. Temperature controls the stability of condensed volatiles on airless planetary bodies. At typical lunar daytime surface temperatures, residence times for H_2O adsorbed to regolith grains are extremely short: for example, < 0.1 ms at 390 K (Hibbitts et al. 2011). Within polar shadows, annual maximum temperatures may be < 100 K, in which case residence time for water molecules is longer than 100 years. In this case, water ice may accumulate if the supply of H_2O outcompetes desorption and other loss processes (see below). Given this range in stability timescales, identifying cold traps for volatiles on the Moon depends upon a detailed knowledge of temperature.

Thermal mapping by the Diviner Lunar Radiometer instrument on the Lunar Reconnaissance Orbiter (LRO) has provided nearly complete maps of annual maximum, minimum, and mean temperatures for both polar regions at a scale of ~250 m (Paige et al. 2010; Williams et al. 2017). Maximum temperatures are most important for determining surface ice stability, given the exponential dependence of sublimation rate on temperature. These data have been used to constrain thermal models (Paige et al. 2010; Siegler et al. 2015, 2016) that can estimate subsurface temperatures. At a depth of ~4 cm, regolith is thermally insulated from the diurnal changes in temperature (Hayne et al. 2017). At this depth, the subsurface temperatures are close to the annual mean surface temperature, which has also been determined by Diviner measurements. The Diviner maps reveal the locations of large-scale cold traps, which are typically defined as regions with annual maximum temperatures < 100–110 K (Paige et al. 2010, see Fig. 13). Although these cold traps follow the pattern of permanent shadows mapped over multi-year timescales by Mazarico et al. (2011), it should be noted that the cold traps are a subset of the PSRs. Temperatures are controlled not only by latitude and shadowing, but also by the detailed and often complex geometry of insolation on surrounding terrain. Therefore, PSRs *may* be cold traps, and indeed are *likely* to be cold traps at latitudes > 80°, but permanent shadow does not guarantee cold-trapping temperatures.

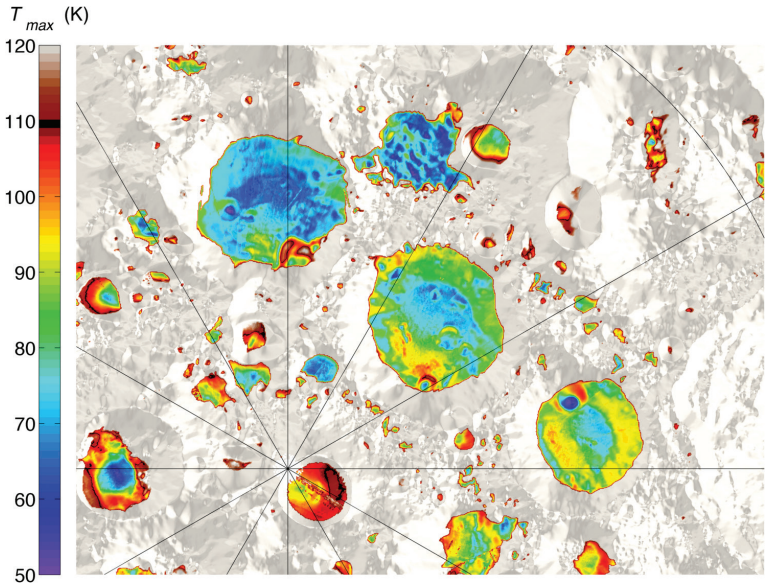

Figure 13. Annual maximum temperature in the south polar region mapped by Diviner. Adapted from Hayne et al. (2015).

3.5.2. Volatile stability. The first estimates of volatile trapping and loss in the lunar PSR date back at least to Watson et al. (1961). This work used equilibrium vapor pressure and an assumed temperature of 120 K to estimate sublimation rates for a number of volatiles at the Moon. Within the last decade, the vapor-pressure-based approach has been widely used to estimate the stability of volatiles expected for a given location on the Moon. The sublimation rate of many volatiles under vacuum as a function of temperature was compiled by Zhang and Paige (2009, 2010) and shown in Figure 2. The vapor-pressure based approach is believed to work well for relatively-pure, bulk deposits of a volatile solid, and is predictive of locations interpreted as bulk water-ice in the PSRs at the North pole of the planet Mercury (Paige et al. 2013). However, when deposits are not pure, or when sub-monolayer quantities of a volatile are adsorbed on the surface of a different material, the assumed energetics of a volatile-on-its-own-ice model break down. It has been shown that volatiles deposited on water ice can be retained at temperatures well above those predicted by the above model approach (e.g., Collings et al. 2003). Trapping of volatiles in a water-ice matrix is one possible explanation for detection of the 'super volatiles' methane and carbon monoxide during the LCROSS impact experiment (Colaprete et al. 2010; Gladstone et al. 2010).

Moving beyond the PSRs, spectra interpreted as OH have been observed on relatively warm, sunlit locations on the Moon. These observations are being examined in greater detail to rule out instrumentation- and/or model-based systematic errors, however, lab experiments examining the plausibility of water adsorption to lunar regolith under these conditions have also been performed (Hibbitts et al. 2011; Poston et al. 2013, 2015). Poston et al. exposed terrestrial surrogates (2013) and lunar samples (2015) to water molecules in an ultra-high vacuum system and found sub-monolayer quantities of retention of water to temperatures more than double those predicted by vapor-pressure based theory (see Fig. 14). To explain this, Poston et al. (2013, 2015) applied well-established theories from the surface chemistry community that focus on the surface energetics of the adsorbate-adsorbent physical interactions. In this framework, desorption probability is described by the Polanyi–Wigner equation

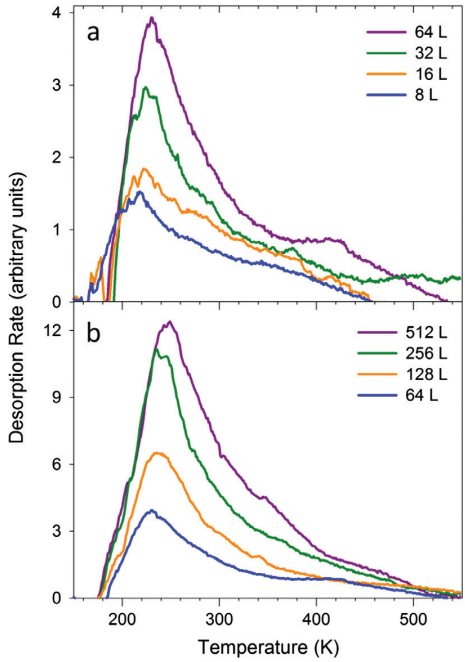

Figure 14. Laboratory experiments of water desorption from lunar regolith samples show the temperature dependence of the desorption rate and how it changes as a function of the amount of water coverage on the soils. [Reproduced from Poston et al. (2015).]

(e.g., Poston et al. 2013). In the case of a heterogeneous lunar soil it was found that the best way to explain the observed desorption measurement was with a superposition of desorption from surface sites with a distribution of adsorption energy values. This reflects the fact that at the nanometer scale each location on the surface of a grain will have different potentials based on proximity to chemical and topographic features of the surface. The implication is that models of volatile stability and surface lifetimes for locations of sub-monolayer coverage (i.e., most of the lunar surface) should have improved predictive power if they include a distribution of volatile-surface interactions with greater strength than those implied by volatile-on-its-own-ice interactions (Farrell et al. 2015, 2017)

3.4.3. Orbital evolution effects on thermal stability. Two main orbital parameter changes could affect stability of ice on the Moon: variations in lunar obliquity and true polar wander. Ward (1975) predicted large changes in lunar obliquity as the Moon slowly receded from the Earth. While we do not yet have a time scale constraint on the growth rate of the lunar semimajor axis (Bills 1999; Siegler et al. 2011, 2015), we can use thermal models to identify where ice would be stable under past obliquities. Arnold (1979) and later work (Paige et al. 2010; Siegler et al. 2015) predicted that lunar cold traps capable of storing water ice would disappear at greater than about 12° obliquity, which last occurred on the Moon anywhere between ~2 and 4 billion years ago, with obliquity getting progressively lower since (and ice becoming more stable). Ancient deposition of ice under higher obliquity could explain some of the paucity of ice compared to models of present-day ice stability predictions.

True polar wander (physical movement of the spin axis relative to lunar surface features) has also been suggested as a reason for the paucity and longitudinal bias in hydrogen as identified by neutron spectroscopy (Miller et al. 2014; Siegler et al. 2016). Large events such as basin formation (Keane and Matsuyama 2014) or internal thermal evolution (Siegler et al. 2016) could move the lunar spin axis by several degrees. A component of water ice delivered when the spin axis shifted by approximately 6 degrees along the 145–215° E longitudes has been found to most strongly correlate with epithermal neutron data. This correlates well with predicted direction and magnitude of spin axis motion due to the thermal evolution of the Procellarum KREEP Terrain region (Laneuville et al. 2013; Siegler et al. 2016).

3.6. Migration

Once on the surface, volatiles are redistributed through the lunar environment via a number of processes. A localized process is the diffusion through the porous regolith, while the collisionless exosphere allows the volatiles to migrate from one place to another covering considerable distances. Finally, impact gardening can change dramatically the spatial distribution of volatiles.

3.6.1. Migration/hopping in the exosphere. Once released in the exosphere, volatiles travel in ballistic trajectories. Most of the atoms and molecules will return to the surface at a considerable distance from the point of ejection. Low-mass volatiles ejected by the most energetic processes (e.g., micrometeoroid impact vaporization) will instead escape into space. Because of the tenuous nature of the exosphere, collisions among particles are extremely rare, and the ensuing ballistic trajectories can be modelled easily. Recent works have benefited from the advancement in the computational capabilities of modern processors, and exospheric modeling can now help explaining the fate of lunar surface volatiles like argon (Grava et al. 2015), water (Moores 2016; Schorghofer et al. 2017), and sodium (Tenishev et al. 2013) and where they are preferentially deposited. The interest in modeling such environment arises from the fact that, traveling through the exosphere, volatiles ejected at low latitudes can reach the poles and become cold-trapped. More detail is provided in Farrell et al. (2023, this volume). Whether exospheric migration of water is an efficient mechanism for delivering water to the cold traps remains an open question. Many unanswered questions regarding the initial release mechanisms, the quantity of water

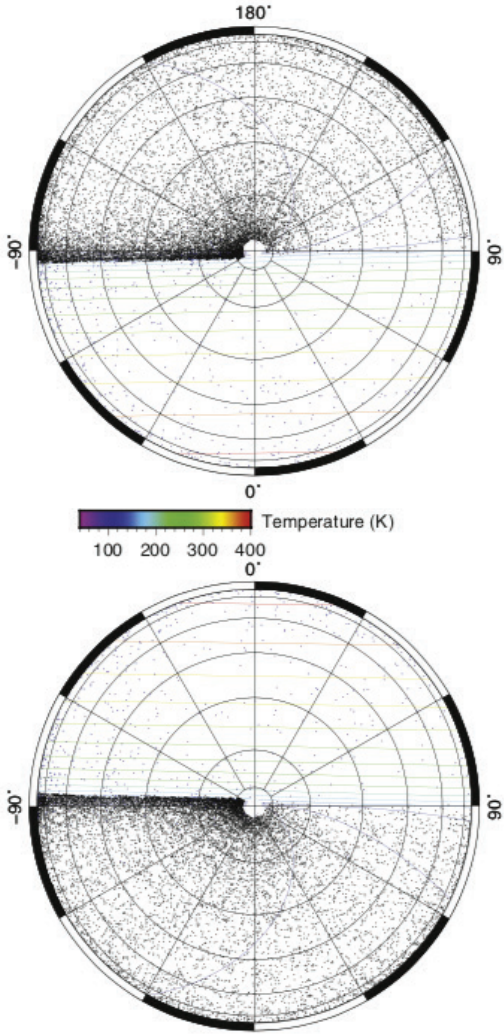

Figure 15. Model output of the position of water molecules on the surface of the Moon for a migrating exosphere of water. [Reproduced from Schorghofer et al. (2017).]

released, and the interaction between water molecules and the surface that preclude quantifying water delivery to the cold traps through the exosphere. However, the low abundance of water in PSRs and the heterogeneous distribution of exposed ice in PSRs suggests that exospheric migration is either inefficient or is counteracted by a strong loss process.

Exospheric migration has been proposed as an explanation for changes in the surface hydration signature on timescales shorter than a lunation. Exospheric migration has been observed in Ar (e.g., Hodges 1975) in which Ar becomes progressively more stably stuck to the nightside surface as the temperature decreases throughout the lunar night and is released back into the exosphere as it reaches the dawn terminator. If water behaves similarly, the distribution of water on the surface of the Moon should exhibit a local time dependence (see Fig. 15). Depending on the sticking properties used, models predict the greatest density on the morning side of the Moon, a depletion at noon, and a gradual increase after sunset (Schorghofer et al. 2017). As understanding of the surface hydration observations improves, it will be possible to compare those to exospheric migration model predictions.

Both NMS and UVS on LADEE and Lunar-based Ultraviolet Telescope (LUT) on the Chang'e-3 lander searched for the ambient, migrating water exosphere on the Moon. The LUT placed an upper limit on OH in the exosphere at $< 10^4$ cm^{-3} (Wang et al. 2015). NMS measurements have placed an upper limit of 0.6 cm^{-3} (Benna et al. 2019) based on many measurements at the instrument background level. However, sporadic detections of exospheric water have been observed and attributed to meteoroid impact release of water (Benna et al. 2019). The existing data cannot uniquely determine the amount of this water that promptly escapes the Moon and how much returns to potentially migrate to the poles. However, the present upper limit of the ambient water exosphere is not consistent with a large source rate of water to the exosphere and efficient migration. Therefore, it is expected that either water does not take many hops in the exosphere before it is lost or solar wind hydrogen is not converted to water as a primary pathway.

3.6.2. Migration/diffusion through regolith. Unless an atom or molecule resides in a Permanently Shaded Region (PSR), it is subject to a certain degree of lateral and vertical mobility across the regolith. In fact, the regolith itself is formed by loosely packed grains which form high porosity fairy-castle-like structure (Hapke and van Horn 1963), where particles undergo multiple collisions before being released into the exosphere (Hodges 2011). Sarantos et al. (2010) have shown that particularly energetic ions (such as those of the solar wind) can favor the diffusion of sodium atoms upwards to the surface, an effect which is visible as enhancements in ground-based observations of lunar sodium exosphere after passages through the Earth's plasma sheet and the consequent encounter with energetic ions (Wilson et al. 2006).

Work is ongoing to understand the rates of diffusion of solar wind implanted hydrogen within a grain of regolith, as well as from one regolith grain to another (Starukhina and Shkuratov 2000; Starukhina 2001, 2003, 2006; Farrell et al. 2015, 2017). Laboratory experiments of proton bombardment of targets reach saturation with fluences of ~ 10^{17} cm^{-2} (e.g., Mattern et al. 1976). On the Moon, this saturation fluence can be reached in 100 years, which is a short time compared to the exposure time of regolith grains on the surface. Whether the diurnal signature represents the difference in the steady-state balance between the diffusion rate and the incident flux as a function of surface temperature or if significant buildup of solar wind implanted hydration occurs over multiple lunations is still unresolved.

Vertical migration of ice within the regolith has been a common theme in many recent research advances. Ice will be inherently more stable if buried by even a small layer of regolith. Burial by even a thin (a few cm) regolith cover will both thermally insulate a buried volatile and inhibit diffusion. The general formalism for this is discussed in Schorghofer and Taylor (2007) with loss rates depending on modeled subsurface temperature (e.g., Paige et al. 2010) and regolith grain size. This has been applied in several papers with an assumed ~ 75 μm grainsize (e.g., Paige et al. 2010; Siegler et al. 2015, 2016) to predict the depth at which water ice should be stable under current lunar orbital conditions.

The area where near-surface water ice could be stable increases by an order of magnitude to 240,000 km^2 compared to the area where surface ice is stable. Detected ice deposits on Mercury strongly match such predictions (e.g., Paige et al. 2013). Departures from this stability map imply at least one of the following: that water ice on the Moon is a supply limited process, that there is a bias in existing measurements, or that ice is very ancient, potentially delivered under past orbital conditions.

In addition to outward movement, Schorghofer and Taylor (2007) and Schorghofer and Aharonson (2014) have shown that, where the surface temperature is favorable, downward migration of water (the thermal pump) allows for subsurface reservoirs of water when there is none at the surface (see Fig. 16). Plentiful regions exist on the Moon where water ice and other volatiles might not be stable on the surface, but are stable in the near subsurface. If temperature and vapor supply conditions favor downward migration, surface water can reach these more stable reservoirs. However, when surface supply is removed, this deeper ice can be lost at a similar rate to that at which it was deposited (Schorghofer and Taylor 2007).

3.7. Photodesorption/dissociation and electron-stimulated desorption

Ultraviolet light can also provide the energy to release molecules from the surface of the Moon in a process known as photon-stimulated desorption (PSD). The Sun is the greatest source of UV for the Moon, thus the dayside is subjected to PSD. The effects of PSD have been observed via sodium, a volatile that is primarily released by PSD (Wilson et al. 2003, 2006; Killen et al. 2004).

In PSRs, there is no direct sunlight. However, there are other illumination sources to PSRs in the UV, including starlight, Earthshine, and zodiacal light (Morgan and Shemansky 1991).

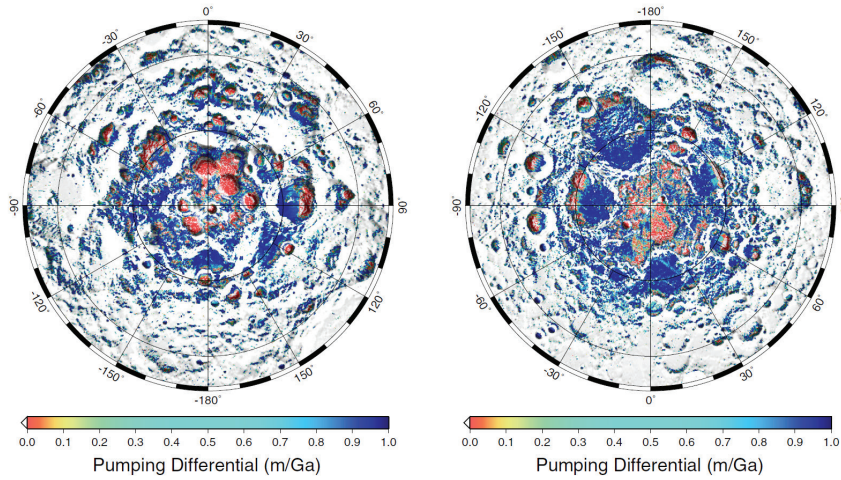

Figure 16. Model of thermal pumping shows locations in the lunar polar regions where thermal cycling is efficient in transporting volatiles from the unstable layer at the surface to the subsurface, where they are more stable against sublimation loss. [From Schorghofer and Aharonson (2014), reproduced by permission of the AAS]

Photodesorption measurements of water deposited on lunar samples have been measured in the lab (DeSimone and Orlando 2014a,b, 2015; Poston et al. 2015; Hibbitts et al. 2011), as well as monolayer coverages deposited on carbon films (Mitchell et al. 2013). However, this process is only effective on molecules exposed to light. Thus, a thin ejecta layer can protect water and other volatiles from PSD in PSRs.

4. OUTSTANDING QUESTIONS AND DATA NEEDED

This chapter has presented the current understanding of lunar surface volatiles in terms of what is known about the amounts and distribution of volatiles on the Moon and what is known about the important physical processes acting to control the volatiles. In this section, we discuss the future directions of the field of research.

4.1. Inventory of lunar volatiles

A high priority goal for lunar volatiles is to develop a complete inventory of lunar volatiles, i.e., a complete assessment of the abundance, composition, distribution, and physical form of volatiles on the Moon. This is important in order to aid in the scientific understanding of the lunar volatiles system and to enable use of volatiles on the Moon as a resource for exploration. The data in hand has been well-explored, still innovative analyses and integration of those data continue to add to the state of knowledge of the lunar volatile inventory. Outstanding questions that should be addressed with the existing data include how to reconcile different orbital measurements with different sensitivities. These can be used to differentiate between volatile deposits that persist through depth or that are limited to a surface expression.

Ultimately, additional data are needed to complete the inventory. Of great interest are global hydration data that can be interpreted without the ambiguities that presently exist with the phase function and thermal corrections. In addition, these data should have spatial and temporal resolution to separate local time effects from compositional differences. These will show to what degree a diurnal hydration cycle exists on the Moon and provide insight into the interaction between hydration and regolith grains. Remote sensing data of the polar regions can define

the scales and degrees of heterogeneity of the lunar cold traps. Active experiments that detect spectroscopic properties of the material in shadowed regions can determine the composition.

Further characterization of the lunar exosphere is important because the exosphere is comprised of volatiles, and because it provides evidence of surface-volatile interactions, source rates, migration, and sinks. While LADEE provided much-needed data from the equatorial region, more measurements from mid latitude and the polar regions are required, as are more comprehensive searches for species.

While mapping data of higher spatial resolution are also needed for the lunar polar regions, in situ data from the PSRs, illuminated polar regions, and other regions of interest such as magnetic anomalies are highly desired. Single point measurements may be used to glean information about composition, isotopic abundances that can provide links to sources, and physical form. Both inside and outside of PSRs, in situ measurements of regolith properties including grain size distributions are critical for interpretation of remote sensing data.

Multipoint measurements, however, will lead to huge advances in understanding. Because of the known heterogeneity of PSR volatiles, multi-point measurements, especially if they can be obtained on traverses that cover scales from decimeters to kilometers, quantify the overall distribution. These measurements should investigate not only the lateral distribution, but also the depth distribution. Only then can ground truth for orbital measurements be applied. The relationship between the distribution and other physical characteristics can be used to determine which processes, sources, and sinks are the most influential in determining the distribution.

4.2. Age of deposits

The historical flux of volatiles to the Moon is more than adequate to supply the present contents of the PSRs. Because the PSRs are not filled to capacity with volatiles, loss processes must be extremely effective on the Moon. Perhaps the Moon cannot build up a deposit. In that case, it is plausible that the volatiles in lunar PSRs represent the steady state balance between ongoing source and loss mechanisms, implying that the contents are young. However, if the steady state balance dominates the current contents, then it is difficult to understand the heterogeneous distribution of volatiles that does not correspond unilaterally to temperature or any other organizing factor. On the other hand, if ongoing losses effectively cancel out the ongoing sources, then the PSR volatiles may be residuals from one or more episodic events. Impact gardening modeling suggests that the depth distribution and the abundance are consistent with a deposit between 500–1000 Ma (Hurley et al. 2012b). While this fits in well with the heterogeneous distribution, it is difficult to understand why Mercury's PSRs are full and the Moon's PSRs are not except the chance encounter of a very recent comet impact on Mercury or more efficient production of water at Mercury (Jones et al. 2018). Siegler et al. (2016) suggest that the present distribution of hydrogen observed by neutron spectrometry is consistent with ancient deposits at a time when the poles were positioned elsewhere. Subsequent polar wander shifted the positions of the PSRs, and despite losses, this hydrogen-rich material appears to make up roughly half of the current neutron suppression signal (best fit by a 57% current, 43% pre-wander mixture). It is unclear that all the craters potentially harboring ground ice pre-existed these historic orbital changes. This is both because the dates of these events and many polar craters are not yet well constrained, but also that data resolution does not currently allow precise localization of neutron suppressing regions. Efforts towards all of these constraints are currently underway.

Many new measurements can be made to help resolve the age of the polar deposits. First, measurements of the composition of volatiles including the isotopic composition will constrain the possible sources, which naturally relate to an age. Second, quantification of the present-day balance of sources and losses will determine the amount of the current contents that can be

attributed to ongoing sources. Third, measurement of the depth distribution over 1–3 m and the lateral heterogeneity of the contents on 10–1000 m scales will relate to an age through impact gardening. In parallel, efforts in theory and numerical modeling need to continue. Models provide the link in understanding from the observation to the processes that produce the observation.

4.3. Relative importance of sources and sinks

Is the Moon presently in a state of accumulation, loss, or balance of its volatiles? This is a relatively basic question, yet we do not currently have the information needed to answer it. In fact, one must also factor in a timescale for the consideration of the question, as we know that over the history of the Moon, there is a net accumulation of volatiles in the PSRs.

The sources of volatiles to the Moon operate on different timescales. Thus, the ongoing sources of solar wind and meteoroid bombardment may dominate the present source rate, but they may not be the greatest source when integrated over time. To address the relative importance of the sources, identification of the isotopic composition of the volatiles in PSRs will determine where the volatiles came from, and thus the original source of the volatiles. In addition, while we cannot go back in time to quantify the source rates from episodic events such as comet impacts and volcanic releases, we can quantify the rate of ongoing sources of volatiles. We can examine the interaction of the solar wind with the surface of the Moon to determine the efficiency of H_2O production. We can observe the impact vapor plumes from meteoroid impacts to determine the retention rate of volatiles delivered or released by meteoroid impacts.

Many of the ongoing sinks can also be measured directly. For example, a monitor on the rim of a PSR can detect outgoing volatiles to quantify the loss rate of volatiles expelled from the PSRs and how they vary according to illumination conditions and temperature, incident meteoroid flux, and solar wind access. Likewise, high resolution, long-term monitoring of surface volatiles can detect changes in the amounts and distribution to constrain the loss processes acting on the extreme surface. It would be particularly interesting to identify a recently exposed ice layer in a lunar PSR and to monitor its evolution over time.

An active experiment would be an exciting and efficient way to characterize the lifecycle of lunar volatiles. As exploration of the Moon continues, landed missions will introduce known quantities of volatiles in a controlled manner to the Moon. Watching the evolution of those volatiles with existing assets or with experiments specifically designed to monitor gas releases on the Moon can provide direct tests of migration, surface interactions and loss rates of volatiles.

Laboratory experiments are critical to understanding the interactions between volatiles and regolith. Continued experiments to reproduce the solar wind interaction with regolith, to quantify the stability of volatiles in a lunar environment, and to provide reference measurements for comparing spacecraft data will enable better modeling and data analysis. With additional Apollo samples being opened and made available for analysis, a great improvement can be made to interpretation of existing data.

4.4. In situ resource utilization and accessibility

Water and other volatiles are potentially usable resources for exploration (see Crawford et al. 2023, this volume). An economically viable "ore" or "reserve" must have sufficient abundance in a sufficiently manageable space for economic exploitation. For example, the recovery of sufficient water for separation into 10,000 kg of oxygen for crew use requires sufficient abundance (>0.5 wt.%) in a workable area ($<100 \times 100$ m), with a sufficiently shallow depth distribution (<0.5 m depth) due to the cost/difficulty of overburden removal. In the end, for in situ resource utilization, there are specific requirements on the knowledge of the composition and physical state, abundance, and lateral and vertical distribution that must be addressed in order to gauge the strategic and economic accessibility and value of such resources.

A variety of measurements addressing both composition and physical state are possible, but a key requirement is a landed, mobile mission. LCROSS demonstrated that there are indeed volatile chemical compounds present at one very cold, permanently-shadowed location. But the physical form of water (massive ice in slabs vs. finely disseminated grains in the regolith) and other compounds remains poorly constrained. Prospecting by its nature requires a continuous characterization of a potential resource over a potential recovery area. We do not understand the sources, physical processes and resulting scales governing the current distribution of, for example, water ice. Equally frigid, equally dark cold traps appear to have retained very different amounts of hydrogen-bearing species, for example. Assaying volatile composition and physical form of subsurface samples acquired during a traverse over scales of 100s of meters to kilometers will greatly improve understanding of the compounds, and their physical forms, that are sequestered in different thermodynamic and geologic settings. These subsurface sample measurements will be tied to surface instrument data acquired continuously during the traverse and will be the first steps to creating an economic mineral model for commercial use.

4.5. Comparisons with analogous bodies

The most prevalent kind of body in the Solar System is a rocky body that is exposed to the harsh space environment without protection from an atmosphere or magnetic field. Many of the asteroids and moons are likewise exposed. The proximity of the Moon makes it an excellent case study for rocky bodies in the Solar System, and many of the lessons regarding volatiles can be applied to asteroids, Mercury, and other Moons. However, there are important differences as well that can be exploited to examine how properties such as temperature, magnetic fields, gravity, impact velocity, and composition influence the evolution of volatiles.

4.5.1. Mercury. Similar to the Moon, Mercury also has PSR that are capable of hosting ice. Models suggest that these cold traps are thermally stable environments for near-surface and sometimes surface water ice on geologic timescales (Paige et al. 2013). Earth-based radar observations of Mercury first revealed highly reflective materials that are consistent with water ice (Harmon and Slade 1992; Slade et al. 1992; Butler et al. 1993; Harmon et al. 2001). Enhanced concentrations of hydrogen were subsequently detected in the north polar region (Lawrence et al. 2013). The surface reflectance of the ice deposits is anomalously lower or higher than the average reflectance of Mercury (Neumann et al. 2013); the low-reflectance deposits are interpreted to be thin layers of volatiles and organics that help insulate the water ice beneath it (Paige et al. 2013), while the high-reflectance deposits are interpreted to be exposed water ice (Neumann et al. 2013; Chabot et al. 2014) (see Fig. 17).

While both Mercury and the Moon have permanently shadowed terrain that contains enhancements in volatiles, there are important differences that need to be explained. The polar craters at Mercury appear to have at least several-meters-thick reservoirs of water ice (Harmon 2007), whereas radar data for the Moon do not conclusively indicate a coherent layer of ice within the upper few meters of the regolith at lunar PSRs (Lawrence 2017; Fassett et al. 2019).

Furthermore, the ice at Mercury is very pure, and analysis of Earth-based radar data indicates the ice deposits are nearly pure water ice and have less than ~5% volume fraction of silicates (Butler et al. 1993), whereas the ice/hydrogen on the Moon appears to be more mixed with regolith (e.g., Gladstone et al. 2012; Li et al. 2018).

In addition, the spatial distribution of ice on Mercury correlates well with the thermal models. The exposed ice exists only in the coldest locations, whereas the ice covered by dark lag deposits occurs in slightly warmer areas (Paige et al. 2013). However, not all of Mercury's cold traps contain ice according to radar measurements (Deutsch et al. 2016). So, while the cold traps with large quantities of volatiles correspond to thermal stability, an additional process is acting such that some of Mercury's PSRs do not exhibit large quantities of ice.

Surface chemistry involving solar wind protons is expected to play a role in the production of water at the Moon, although the efficiency and dependencies of the process are not well-known. The solar wind also interacts with the surface of Mercury and could produce water there as well. However, Mercury's magnetosphere modifies the spatial distribution and energetics of the incident ion flux compared to the Moon. On Mercury, ion precipitation on the surface is enhanced at mid-high latitudes, where the magnetic field cusps provide direct access for incident solar wind. Confirmation of this comes from ground-based observations showing sporadic high-latitude enhancements of sodium in Mercury's exosphere often attributed to sputtering (Mangano et al. 2013). Thus, water produced from the solar wind interaction begins closer to the cold traps, and migration to the cold traps may be more efficient. However, there is expected to be a greater ion flux directly into the cold traps themselves which makes sputtering a more efficient erosion mechanism for Mercury than the Moon.

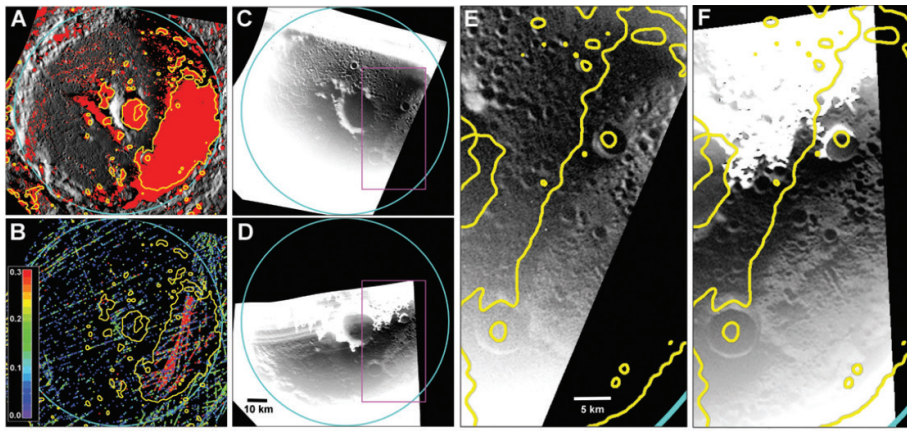

Figure 17. MESSENGER images inside Mercury's PSRs reveal a bright deposit coinciding with the area in permanent shadow and the location of the radar-bright signal. [Reproduced from Chabot NL, Ernst CM, Denevi BW, Nair H, Deutsch AN, Blewett DT, Murchie, SL Neumann GA, Mazarico E, Paige DA, Harmon JK, Head JW, Solomon SC (2014) Images of surface volatiles in Mercury's polar craters acquired by the MESSENGER spacecraft. Geology 42:1051–1054 with permission from the Geological Society of America.]

Yet, the absolute flux of ions to the surface of Mercury and the energy distribution is hard to quantify with existing data. The energy of the ions governs the depth of implantation and the sputtering yield. Therefore, the Moon may offer a way to understand how the process works at Mercury. The Moon has local magnetic anomalies that interact with the solar wind to shield the surface in some regions (Wieser et al. 2010; Poppe et al. 2017) and act as cusps that provide access to the surface in other regions. As understanding of the relationship between ion fluxes and water production improve on Mercury or the Moon, the lessons can be applied to the other body.

The role of meteoritic impact has been shown to be an important, if not dominant, source of exospheric atoms at both Mercury (Killen and Hahn 2015) and the Moon (Colaprete et al. 2016; Hurley et al. 2017; Benna et al. 2019). However, the rate of impact vaporization is highly dependent on the flux of interplanetary dust onto the bodies and their velocity distributions. Both of these parameters, density and velocity, are still to a large extent uncertain at both Mercury and the Moon. Although the expected flux of impactors is expected to be lower on Mercury than on the Moon, the impactors dynamically should have a higher relative velocity on Mercury, and therefore impart more energy into the system on Mercury than the Moon (Cintala 1992). Bruck Syal et al. (2015) calculated the delivery rate of carbon-bearing species to Mercury from micrometeoroids and comets and find the micrometeoroids are both a stronger source of exogenous carbon and less susceptible to escape. Crider and Killen (2005) investigated the erosion rate of an ice layer

on Mercury due to impact gardening. The faster gardening rate on Mercury leads to a more rapid burial of ice deposits on Mercury compared to the Moon, assuming that thermal processes do not redistribute the ice. The coherent nature of the ice deposits on Mercury suggests that they are either younger than ~100 Ma or impact gardening occurs at a slower pace than thought, or thermal processes are effective at concentrating the ice on Mercury.

The pervasive nature of thick deposits on Mercury compared to the patchy, low-abundance, water–soil mixtures on the Moon suggests vastly different processes occur on the two nominally similar bodies. Whether the answer is a recent large comet impact onto Mercury, other more pervasive sources, more efficient transport, or effective retention on Mercury is a topic of much future work.

4.5.2. Asteroids. Asteroids are similar to the Moon in that they are exposed to the space environment. Asteroids are known to have a diversity of compositions which are modulated in part by their heliocentric distance and by whether they were large enough to differentiate. Hydration features on 4-Vesta have been observed both using ground-based telescopes (Hasegawa 2003) and from the Dawn spacecraft (DeSanctis et al. 2012). Dawn observations demonstrate a heterogenous distribution of the 2.8–3.0 μm line with strongest signatures related to the older terrains. The heterogeneous distribution implies that solar wind implantation and continuous infall from meteoroids do not play a significant role; and place the source to a time in the past that predates the large impact features on Vesta.

Dwarf planet Ceres orbits at a distance of ~2.8 AU, where daytime temperatures of up to ~240 K preclude water ice on the sunlit surface. However, ice would be stable in the near subsurface over much of the body (Fanale and Salvail 1989). Furthermore, Ceres' present-day low obliquity of ~4° leads to ~0.1% of the surface being occupied by perennial shadows with maximum temperatures predicted to be far below the ~110-K threshold for water ice sublimation (Schorghofer et al. 2016). With a water-rich crust (McCord and Sotin 2005) and a transient water exosphere (Küppers et al. 2014), models based on classical cold-trapping theory predicted net accumulation of water and other volatiles in the polar cold traps (Hayne and Aharonson 2015). Therefore, NASA's Dawn mission had the opportunity to test theories widely applied to lunar polar volatiles, on a similar body.

In its polar orbit about Ceres, Dawn used scattered light imaging to detect bright patches inside some, but not all of the PSRs, which were inferred to be ice deposits (Platz et al. 2016). This observation is unexpected for an isotropic source (e.g., ballistic hopping), which would contribute to all cold traps equally. However, Ermakov et al. (2017) showed that obliquity variations up to ~20° lead to differential shadowing during the 24.5-kyr cycle, which may explain the apparent differences in PSR ice content. In this case, the supply rate of water to Ceres' polar regions should be too low to form an optically thick frost on timescales <24.5 kyr. Rather, only those PSRs that survive to 20° obliquity would have the opportunity to accumulate a frost layer. Survival of such a layer also depends on local rates of loss processes (sputtering, photodestruction, gardening) known to occur on the Moon. One key difference in the observed ice distribution between these two bodies is that those on Ceres are relatively contiguous within their host PSRs as they are on Mercury, whereas ice on the Moon appears to be much patchier. This may indicate a lower supply rate on the Moon compared to the destruction or gardening processes.

5. CONCLUSIONS

The new view of lunar surface volatiles is that the Moon is not a dry, desolate world. Instead, the Moon has a history of volatiles from its formation, through ancient outgassing events, more recent impacts of volatile rich bodies, and the ongoing interaction with the space

environment. Furthermore, the Moon contains an accessible record of these processes on its surface, especially in PSR. As our understanding of the processes acting on the Moon now and previously improves, these lessons can be carried on to improve the understanding of the way airless bodies interact with the space environment. They can quantify the sources of volatiles to the inner Solar System. Furthermore, they can inform the potential usage of volatiles on the Moon and other bodies as a resource for exploration.

REFERENCES

Anders E (1964) Origin, age, and composition of meteorites. Space Sci Rev 3:583–714

Arnold JR (1975) A Monte Carlo model for the gardening of the lunar regolith. Moon 13:159–172

Arnold JR (1979) Ice in the lunar polar regions. J Geophys Res 84(B10):5659– 5668

Artemieva NA, Shuvalov VV (2008) Numerical simulation of high-velocity impact ejecta following falls of comets and asteroids onto the Moon. Sol Sys Res 42:329–334

Bandfield JL, Poston MJ, Klima RL, Edwards CS (2018) Widespread distribution of OH/H_2O on the lunar surface inferred from spectral data. Nat Geosci 11:173–177

Barnes JJ, Kring DA, Tartèse R, Franchi IA, Anand M, Russell SS (2016) An asteroidal origin for water in the Moon. Nat Commun 7:11684

Benna M, Mahaffy PR, Halekas JS, Elphic RC, Delory GT (2015) Variability of helium, neon, and argon in the lunar exosphere as observed by the LADEE NMS instrument. Geophys Res Lett 42:3723–3729

Benna M, Hurley DM, Stubbs TJ, Mahaffy PR, Elphicy RC (2019) Lunar soil hydration constrained by exospheric water liberated by meteoroid impacts. Nat Geosci 12:333–338

Beran A, Rossman GR (2006) OH in naturally occurring corundum. Eur J Mineral 18:441–447

Berezhnoy AA (2013) Chemistry of impact events on the Moon. Icarus 226:205–211

Besserer J, Nimmo F, Wieczorek MA, Weber RC, Kiefer WS, McGovern PJ, Andrews-Hanna JC, Smith DE, Zuber MT (2014) GRAIL gravity constraints on the vertical and lateral density structure of the lunar crust. Geophys Res Lett 41:5771–5777

Bills BG, Ray RD (1999) Lunar orbital evolution: A synthesis of recent results. Geophys Res Lett 26:3045–3048

Bockelee-Morvan, D, Crovisier J, Mumma MJ, Weaver HA (2004) The composition of cometary volatiles. *In:* Comets II. Keller HU, Weaver HA (eds). Tucson, University of Arizona Press, p 391–424

Boyce JW, Liu Y, Rossman GR, Guan Y, Eiler JM, Stolper EM, Taylor LA (2010) Lunar apatite with terrestrial volatile abundances. Nature 466:466–469

Broadfoot AL, Shemansky DE, Kumar S (1976) Mariner 10: Mercury atmosphere. Geophys Res Lett 3:577–580

Bruck Syal M, Schultz PH (2015) Cometary impact effects at the Moon: Implications for lunar swirl formation. Icarus 257:194–206

Burke DJ, Dukes CA, Kim JH, Shi J, Famá M, Baragiola RA (2011) Solar wind contribution to surficial lunar water: Laboratory investigations. Icarus 211:1082–1088

Butler BJ, Muhleman DO, Slade MA (1993) Mercury: Full-disk radar images and the detection and stability of ice at the north pole. J Geophys Res 98(E8):15003–15023

Campbell DB, Campbell BA, Carter LM, Margot JL, Stacy NJ (2006) No evidence for thick deposits of ice at the lunar south pole. Nature 443:835–837

Carpenter J, Fisackerly R, Houdou B (2016) Establishing lunar resource viability. Space Policy 37:52–57

Chabot NL, Ernst CM, Denevi BW, Nair H, Deutsch AN, Blewett DT, Murchie, SL Neumann GA, Mazarico E, Paige DA, Harmon JK, Head JW, Solomon SC (2014) Images of surface volatiles in Mercury's polar craters acquired by the MESSENGER spacecraft. Geology 42:1051–1054

Cintala MJ (1992) Impact-induced thermal effects in the lunar and mercurian regoliths. J Geophys Res 97(E1):947–973

Clark RN (2009) Detection of adsorbed water and hydroxyl on the Moon. Science 326:562–564

Cocks FH, Klenk PA, Watkins SA, Simmons WN, Cocks JC, Cocks EE, Sussingham JC (2002) Lunar ice: Adsorbed water on subsurface polar dust. Icarus 160:386–397

Colaprete A, Sarantos M, Wooden DH, Stubbs TJ, Cook AM, Shirley M (2016) How surface composition and meteoroid impacts mediate sodium and potassium in the lunar exosphere. Science 351:249–252

Colaprete A, Schultz P, Heldmann J, Wooden D, Shirley M, Ennico K, Hermalyn B, Marshall W, Ricco A, Elphic RC, Goldstein D, Summy D, Bart GD, Asphaug E, Korycansky D, Landis D, Sollitt L (2010) Detection of water in the LCROSS ejecta plume. Science 330:463–468

Collings MP, Dever JW, Fraser HJ, McCoustra MRS (2003) Laboratory studies of the interaction of carbon monoxide with water ice. Astrophys Space Sci 285:633–659

Crawford IA, Anand M, Barber S, Cowley A, Crites S, Fa W, Flahaut J, Gaddis LR, Greenhagen B, Haruyama J, Hurley D, McLeod CL, Morse A, Neal CR, Sargeant H, Sefton-Nash E, Tartèse R (2023) Lunar resources. Rev Mineral Geochem 89:829–868

Crider D, Killen R (2005) Burial rate of Mercury's polar volatile deposits. Geophys Res Lett 32:L12201

Crider DH, Vondrak RR (2002) Hydrogen migration to the lunar poles by solar wind bombardment of the Moon. Adv Space Res 30:1869–1874
Crider D, Vondrak R (2003) Space weathering effects on lunar cold trap deposits. J Geophys Res-Planets 108(E7):5079
Crites ST, Lucey PG, Lawrence DJ (2013) Proton flux and radiation dose from galactic cosmic rays in the lunar regolith and implications for organic synthesis at the poles of the Moon and Mercury. Icarus 226:1192–1200
Crotts APS (2008) Lunar outgassing, transient phenomena, and the return to the Moon. I. Existing data. Astrophys J 687:692–705
De Sanctis MC, Combe JP, Ammannito E, Palomba E, Longobardo A, McCord TB, Marchi S, Capaccioni F, Capria MT, Mittlefehldt DW, Pieters CM, Sunshine J, Tosi F, Zambon F, Carraro F, Fonte S, Frigeri A, Magni G, Raymond CA, Russell CT, Turrini D (2012) Detection of widespread hydrated materials on Vesta by the VIR imaging spectrometer on board the Dawn Mission. Astrophys J 758:L36
Delitsky ML, Paige DA, Siegler MA, Harju ER, Schriver D, Johnson RE, Travnicek P (2017) Ices on Mercury: Chemistry of volatiles in permanently cold areas of Mercury's north polar region. Icarus 281:19–31
DeSimone AJ, Orlando TM (2014a) Mechanisms and cross sections for water desorption from a lunar impact melt breccia. J Geophys Res 119:884–893
DeSimone AJ, Orlando TM (2014b) Photodissociation of water and O(3PJ) formation on a lunar impact melt breccia. J Geophys Res: Planets 119:894–904
DeSimone AJ, Orlando TM (2015) H_2O and O(3PJ) photodesorption from amorphous solid water deposited on a lunar mare basalt. Icarus 255:44–50
DesMarais DJ, Hayes JM, Meinschein WG (1974) The distribution in lunar soil of hydrogen released by pyrolysis. Proc Lunar Sci Conf 5th:1811–1822
Deutsch AN, Chabot NL, Mazarico E, Ernst CM, Head JW, Neumann GA, Solomon SC (2016) Comparison of areas in shadow from imaging and altimetry in the north polar region of Mercury and implications for polar ice deposits. Icarus 280:158–171
Dyar MD, Hibbitts CA, Orlando TM (2010) Mechanisms for incorporation of hydrogen in and on terrestrial planetary surfaces. Icarus 208:425–437
Eke VR, Teodoro LFA, Elphic RC (2009) The spatial distribution of polar hydrogen deposits on the Moon. Icarus 200:12–18
Eke VR, Bartram SA, Lane DA, Smith D, Teodoro LFA (2014) Lunar polar craters—Icy, rough or just sloping? Icarus 241:66–78
Epstein S, Taylor HPJ (1970) The concentration and isotopic composition of hydrogen, carbon and silicon in Apollo 11 lunar rocks and minerals. Proc Apollo 11 Lunar Sci Conf:1085–1096
Ermakov AI, Mazarico E, Schröder SE, Carsenty U, Schorghofer N, Preusker F, Raymond FC, Russell CT, Zuber MT (2017) Ceres's obliquity history and its implications for the permanently shadowed regions. Geophys Res Lett 44:2652–2661
Fa W, Cai Y (2013) Circular polarization ratio characteristics of impact craters from Mini-RF observations and implications for ice detection at the polar regions of the Moon. J Geophys Res Planets 8:1582–1608
Fa W, Eke VR (2018) Unraveling the mystery of lunar anomalous craters using radar and infrared observations. J Geophys Res Planets 123:2119–2137
FanaleFP, Salvail JR (1989) The water regime of Asteroid (1) Ceres. Icarus 82:97–110
Farrell WM, Hurley DM, Hodges RR, Killen RM, Halekas JS, Zimmerman MI, Delory GT (2013) Redistribution of lunar polar water to mid-latitudes and its role in forming an OH veneer. Planet Space Sci 89:15–20
Farrell WM, Hurley DM, Zimmerman MI (2015) Solar wind implantation into lunar regolith: Hydrogen retention in a surface with defects. Icarus 255:116–126
Farrell WM, Hurley DM, Esposito VJ, McLain JL, Zimmerman MI (2017) The statistical mechanics of solar wind hydroxylation at the Moon, within lunar magnetic anomalies, and at Phobos. J Geophys Res: Planets 122:269–289
Farrell WM, Halekas JS, Horányi M, Killen RM, Grava C, Szalay JR, Benna M, Clark PE, Collier MR, Colaprete A, Deca J, Elphic RC, Fatemi S, Futaana Y, Holmström M, Hurley DM, Kramer GY, Mahaffy PR, Nishino MN, Noble SK, Saito Y, Poppe AR, Retherford KD, Wang X, Yokota S (2023) The dust, atmosphere, and plasma at the Moon. Rev Mineral Geochem 89:563–609
Feldman WC (1998) Fluxes of fast and epithermal neutrons from Lunar Prospector: Evidence for water ice at the lunar poles. Science 281:1496–1500
Feldman WC, Lawrence DJ, Elphic RC, Barraclough BL, Maurice S, Genetay I, Binder AB (2000) Polar hydrogen deposits on the Moon. J Geophys Res: Planets 105(E2):4175–4195
Feldman WC, Maurice S, Lawrence DJ, Little RC, Lawson SL, Gasnault O, Wiens RC, Barraclough BL, Elphic RC, Prettyman TH, Steinberg JT, Binder AB (2001) Evidence for water ice near the lunar poles. J Geophys Res: Planets 106(E10):23231–23251
Feldman PD, Hurley DM, Retherford KD, Gladstone GR, Stern SA, Pryor W, Parker JW, Kaufmann DE, Davis MW, Versteeg MH, Team L (2012) Temporal variability of lunar exospheric helium during January 2012 from LRO/LAMP. Icarus 221:854–858
Fisher EA, Lucey PG, Lemelin M, Greenhagen BT, Siegler MA, Mazarico E, Aharonson O, Williams J-P, Hayne PO, Neumann GA, Paige DA, Smith DE, Zuber MT (2017) Evidence for surface water ice in the lunar polar regions using reflectance measurements from the Lunar Orbiter Laser Altimeter and temperature measurements from the Diviner Lunar Radiometer Experiment. Icarus 292:74–85

Gaddis LR, Joy KH, Bussey BJ, Carpenter JD, Crawford IA, Elphic RC, Halekas JS, Lawrence SJ, Xiao L (2023) Recent exploration of the Moon: Science from lunar missions since 2006. Rev Mineral Geochem 89:1–51

Gault DE, Horz F, Brownlee DE, Hartung JB (1974) Mixing of the lunar regolith. Proc Lunar Sci Conf 5th:2365–2386

Gladstone GR, Hurley DM, Retherford KD, Feldman PD, Pryor WR, Chaufray J-Y, Versteeg M, Greathouse TK, Steffl AJ, Throop H, Parker JW, Kaufmann DE, Egan AF, Davis MW, Slater DC, Mukherjee J, Miles PF, Hendrix AR, Colaprete A, Stern SA (2010) LRO-LAMP Observations of the LCROSS Impact Plume. Science 330:472–476

Gladstone GR, Retherford KD, Egan AF, Kaufmann DE, Miles PF, Parker JW, Horvath D, Rojas PM, Versteeg MH, Davis MW, Greathouse TK, Slater DC, Mukherjee J, Steffl AH, Feldman PD, Hurley DM, Pryor WR, Hendrix AR, Mazarico E, Stern SA (2012) Far-ultraviolet reflectance properties of the Moon's permanently shadowed regions. J Geophys Res-Planets 117:E00H04

Gläser P, Oberst J, Neumann GA, Mazarico E, Speyerer EJ, Robinson MS (2018) Illumination conditions at the lunar poles: Implications for future exploration. Planet Space Sci 162:170–178

Goering J, Sah S, Burghaus U, Street KW (2008) Adsorption of water on JSC-1A (simulated moon dust samples)—A surface science study. Surf Interface Anal 40:1423–1429

Gorenstein P, Bjorkholm P (1973) Detection of radon emanation from the crater Aristarchus by the Apollo 15 alpha particle spectrometer. Science 179:792–794

Gorenstein P, Golub L, Bjorkholm P (1974) Radon emanation from the Moon, spatial amd temporal variability. Moon 9:129–140

Granvik M, Morbidelli A, Jedicke R, Bolin B, Bottke WF, Beshore E, Vokrouhlicky D, Delbo M, Michel P (2016) Super-catastrophic disruption of asteroids at small perihelion distances. Nature 530:303–306

Granvik M, Morbidelli A, Vokrouhlický D, Bottke WF, Nesvorný D, Jedicke R (2017) Escape of asteroids from the main belt. Astron Astrophys 598:A52

Grava C, Chaufray J-Y, Retherford KD, Gladstone GR, Greathouse TK, Hurley DM, Hodges RR, Bayless AJ, Cook JC, Stern SA (2015) Lunar exospheric argon modeling. Icarus 255:135–147

Greenwood JP, Itoh S, Sakamoto N, Warren P, Taylor L, Yurimoto H (2011) Hydrogen isotope ratios in lunar rocks indicate delivery of cometary water to the Moon. Nat Geosci 4:79–82

Hapke B, van Horn H (1963) Photometric studies of complex surfaces, with applications to the Moon. J Geophys Res 68:4545–4570

Harmon J (2001) High-resolution radar imaging of Mercury's north pole. Icarus 149:1–15

Harmon JK (2007) Radar Imaging of Mercury. Space Sci Rev 132(2–4):307–349

Harmon JK, Slade MA (1992) Radar mapping of Mercury: Full-disk images and polar anomalies. Science 258:640–643

Hartmann WK, Davis DR (1975) Satellite-sized planetesimals and lunar origin. Icarus, 24:504–515

Hartung JB, Storzer D (1974) Lunar microcraters and their solar flare track record. Proc Lunar Sci Conf 5th:2527–2541

Haruyama J, Ohtake M, Matsunga T, Morota T, Honda C, Yokota Y, Pieters CM, Hara S, Hioki K, Saiki K, Miyamoto H, Iwasaki A, Abe M, Ogawa Y, Takeda H, Shirao M, Yamaji A, Josset J-L (2008) Lack of exposed ice inside lunar south pole Shackleton crater. Science 322:938–939

Hasegawa S (2003) Evidence of hydrated and/or hydroxylated minerals on the surface of asteroid 4 Vesta. Geophys Res Lett 30:2123

Hashizume K, Chaussidon M, Marty B, Robert F (2000) Solar wind record on the Moon: Deciphering presolar from planetary nitrogen. Science 290:1142–1145

Hayne PO, Aharonson O (2015) Thermal stability of ice on Ceres with rough topography. J Geophys Res: Planets 120:1567–1584

Hayne PO, Paige DA, Ingersoll AP, Judd MA, Aharonson O, Alkali L, Byrne S, Cohen B, Colaprete A, Combe JP, Edwards C (2013) New Approaches to Lunar Ice Detection and Mapping: Study Overview and Results of the First Workshop. *In:* Annual Meeting of the Lunar Exploration Analysis Group, Vol. 1748, http://kiss.caltech.edu/final_reports/Lunar_Ice_final_report.pdf

Hayne PO, Hendrix A, Sefton-Nash E, Siegler MA, Lucey PG, Retherford KD, Williams J-P, Greenhagen BT, Paige DA (2015) Evidence for exposed water ice in the Moon's south polar regions from Lunar Reconnaissance Orbiter ultraviolet albedo and temperature measurements. Icarus 255:58–69

Hayne PO, Bandfield JL, Siegler MA, Vasavada AR, Ghent RR, Williams J-P, Greenhagen BT, Aharonson O, Elder CM, Lucey PG, Paige DA (2017) Global Regolith Thermophysical properties of the Moon from the Diviner Lunar Radiometer Experiment. J Geophys Res: Planets 122:2371–2400

Heldmann JL, Lamb J, Asturias D, Colaprete A, Goldstein DB, Trafton LM, Varghese PL (2015) Evolution of the dust and water ice plume components as observed by the LCROSS visible camera and UV–visible spectrometer. Icarus 254:262–275

Hendrix AR, Hansen CJ (2008) Ultraviolet Observations of Phoebe from Cassini UVIS, Icarus 193:323–333

Hendrix AR, Retherford KD, Gladstone GR, Hurley DM, Feldman PD, Egan AF, Kaufmann DE, Miles PF, Parker JW, Horvath D, Rojas PM, Versteeg MH, Davis MW, Greathouse TK, Mukherjee J, Steffl AJ, Pryor WR, Stern SA (2012) The lunar far-UV albedo: Indicator of hydration and weathering. J Geophys Res: Planets 117(E12):E12001

Hendrix AR, Hurley DM, Farrell WM, Greenhagen BT, Hayne PO, Retherford KD, Vilas F, Cahill JT, Poston MJ, Liu Y (2019) Diurnally migrating lunar water: Evidence from ultraviolet data. Geophys Res Lett 46:2417–2424

Hibbitts CA, Grieves GA, Poston MJ, Dyar MD, Alexandrov AB, Johnson MA, Orlando TM (2011) Thermal stability of water and hydroxyl on the surface of the Moon from temperature-programmed desorption measurements of lunar analog materials. Icarus 213:64–72
Hodges RR (1975) Formation of the lunar atmosphere. Moon 14:139–157
Hodges RRJ (1977) Release of radiogenic gases from the Moon. Phys Earth Planet Sci 14:282–288
Hodges RRJ (2002) Ice in the lunar polar regions revisited. J Geophys Res 107(E2):5011
Hodges RR (2011) Resolution of the lunar hydrogen enigma. Geophys Res Lett 38:L06201
Hodges RR (2016) Methane in the lunar exosphere: Implications for solar wind carbon escape. Geophys Res Lett 43:6742–6748
Hodges RR (2018) Semiannual oscillation of the lunar exosphere: Implications for water and polar ice. Geophys Res Lett 45:7409–7416
Hodges RR, Hoffman JH (1974) Measurements of solar wind helium in the lunar atmosphere. Geophys Res Lett 1:69–71
Hodges RR, Mahaffy PR (2016) Synodic and semiannual oscillations of argon-40 in the lunar exosphere. Geophys Res Lett 43:22–27
Holmes HF, Fuller ELJ, Gammage RB (1973) Alteration of an Apollo 12 sample by adsorption of water vapor. Earth Planet Sci Lett 19:90–96
Horányi M, Szalay JR, Kempf S, Schmidt J, Grun E, Srama R, Sternovsky Z (2015) A permanent, asymmetric dust cloud around the Moon. Nature 522:324–326
Horz F, Brownlee DE, Fechtig H, Hartung JB, Morrison DA, Neukum G, Schneider E, Vedder JF, Gault DE (1975) Lunar microcraters: Implications for the micrometeoroid complex. Planet Space Sci 23:151–172
Housley RM, Grant RW, Paton NE (1973) Origin and characteristics of excess Fe metal in lunar glass welded aggregates. Proc Lunar Sci Conf 4th:2737–2749
Hurley DM, Gladstone GR, Stern SA, Retherford KD, Feldman PD, Pryor W, Egan AF, Greathouse TK, Kaufmann DE, Steffl AJ, Parker JW, Miles PF, Horvath D, Davis MW, Versteeg MH, Slater DC, Hendrix AR, Hibbitts CA, Ernst CM, Vervack RJ Jr., Grieves GA (2012a) Modeling of the vapor release from the LCROSS impact: 2. Observations from LAMP. J Geophys Res-Planets 117:E00H07
Hurley DM, Lawrence DJ, Bussey DBJ, Vondrak RR, Elphic RC, Gladstone GR (2012b) Two-dimensional distribution of volatiles in the lunar regolith from space weathering simulations. Geophys Res Lett 39:L09203
Hurley DM, Cook JC, Benna M, Halekas JS, Feldman PD, Retherford KD, Hodges RR, Grava C, Mahaffy P, Gladstone GR, Greathouse T, Kaufmann DE, Elphic RC, Stern SA (2016) Understanding temporal and spatial variability of the lunar helium atmosphere using simultaneous observations from LRO, LADEE, and ARTEMIS. Icarus 273:45–52
Hurley DM, Cook JC, Retherford KD, Greathouse T, Gladstone GR, Mandt K, Grava C, Kaufmann D, Hendrix A, Feldman PD, Pryor W, Stickle A, Killen RM, Stern SA (2017) Contributions of solar wind and micrometeoroids to molecular hydrogen in the lunar exosphere. Icarus 283:31–37
Ichimura AS, Zent AP, Quinn RC, Sanchez MR, Taylor LA (2012) Hydroxyl (OH) production on airless planetary bodies: Evidence from H^+/D^+ ion-beam experiments. Earth Planet Sci Lett 345–348:90–94
Izawa MRM, Cloutis EA, Applin DM, Craig MA, Mann P, Cuddy M (2014) Laboratory spectroscopic detection of hydration in pristine lunar regolith. Earth Planet Sci Lett 390:157–164
Johnson RE (1989) Application of laboratory data to the sputtering of a planetary regolith. Icarus 78:206–210
Johnson RE (2011) Photolysis and radiolysis of water ice. *In:* Physics and Chemistry at Low Temperatures. Khriachtchev L (ed) Singapore, Pan Stanford, p 297–339
Johnson RE, Baragiola R (1991) Lunar surface: Sputtering and secondary ion mass spectrometry. Geophys Res Lett 18:2169–2172
Jones BM, Aleksandrov A, Hibbitts CA, Dyar MD, Orlando TM (2018) Solar wind-induced water cycle on the Moon. Geophys Res Lett 45:10,959–10,967
Jordan AP, Stubbs TJ, Joyce CJ, Schwadron NA, Spence HE, Wilson JK (2013) The formation of molecular hydrogen from water ice in the lunar regolith by energetic charged particles. J Geophys Res Planets 118:1257–1264
Keane JT, Matsuyama I (2014) Evidence for lunar true polar wander and a past low-eccentricity, synchronous lunar orbit. Geophys Res Lett 41:6610–6619
Killen RM, Hahn JM (2015) Impact vaporization as a possible source of Mercury's calcium exosphere. Icarus 250:230–237
Killen RM, Sarantos M, Potter AE, Reiff P (2004) Source rates and ion recycling rates for Na and K in Mercury's atmosphere. Icarus 171:1–19
Killen RM, Potter AE, Hurley DM, Plymate C, Naidu S (2010) Observations of the lunar impact plume from the LCROSS event. Geophys Res Lett 37:L23201
Klima RL, Petro NE (2017) Remotely distinguishing and mapping endogenic water on the Moon. Philos Trans A Math Phys Eng Sci 375(2094):20150391
Klima R, Cahill J, Hagerty J, Lawrence D (2013) Remote detection of magmatic water in Bullialdus Crater on the Moon. Nat Geosci 6:737–741

Kramer GY, Besse S, Dhingra D, Nettles J, Klima R, Garrick-Bethell I, Clark RN, Combe J-P, Head JW, Taylor LA, Pieters CM, Boardman J, McCord TB (2011) M3 spectral analysis of lunar swirls and the link between optical maturation and surface hydroxyl formation at magnetic anomalies. J Geophys Res 116:E00G18

Kuppers M, O'Rourke L, Bockelee-Morvan D, Zakharov V, Lee S, von Allmen P, Carry B, Teyssier D, Marston A, Muller T, Crovisier J, Barucci MA, Moreno R (2014) Localized sources of water vapour on the dwarf planet (1) Ceres. Nature 505:525–527

Laneuville M, Wieczorek MA, Breuer D, Tosi N (2013) Asymmetric thermal evolution of the Moon. J Geophys Res: Planets 118:1435–1452

Lanzerotti LJ, Brown WL, Johnson RE (1981) Ice in the polar regions of the Moon. J Geophys Res 86(B5):3949–3950

Lawrence DJ (2017) A tale of two poles: Toward understanding the presence, distribution, and origin of volatiles at the polar regions of the Moon and Mercury. J Geophys Res: Planets 122:21–52

Lawrence DJ, Hurley DM, Feldman WC, Elphic RC, Maurice S, Miller RS, Prettyman TH (2011) Sensitivity of orbital neutron measurements to the thickness and abundance of surficial lunar water. J Geophys Res 116(E1):E01002

Lawrence DJ, Feldman WC, Goldsten JO, Maurice S, Peplowski PN, Anderson BJ, Bazell D, McNutt RL, Nittler LR, Prettyman TH, Rodgers DJ, Solomon SC, Weider S (2013) Evidence for water ice near Mercury's north pole from MESSENGER Neutron Spectrometer measurements. Science 339:292–296

Lawrence DJ, Peplowski PN, Plescia JB, Greenhagen BT, Maurice S, Prettyman TH (2015) Bulk hydrogen abundances in the lunar highlands: Measurements from orbital neutron data. Icarus 255:127–134

Lawson SL, Feldman WC, Lawrence DJ, Moore KR, Elphic RC, Belian RD, Maurice S (2005) Recent outgassing from the lunar surface: The Lunar Prospector Alpha Particle Spectrometer. J Geophys Res 110(E9):E09009

Li S, Milliken RE (2016) An empirical thermal correction model for Moon Mineralogy Mapper data constrained by laboratory spectra and Diviner temperatures. J Geophys Res 121:2081–2107

Li S, Lucey PG, Milliken RE, Hayne PO, Fisher E, Williams JP, Hurley DM, Elphic RC (2018) Direct evidence of surface exposed water ice in the lunar polar regions. Proc Natl Acad Sci 115:8907–8912

Liu Y, Guan Y, Zhang Y, Rossman GR, Eiler JM, Taylor LA (2012) Direct measurement of hydroxyl in the lunar regolith and the origin of lunar surface water. Nat Geosci 5:779–782

Livengood TA, Chin G, Sagdeev RZ, Mitrofanov IG, Boynton WV, Evans LG, Litvak ML, McClanahan TP, Sanin AB, Starr RD, Su JJ (2015) Moonshine: Diurnally varying hydration through natural distillation on the Moon, detected by the Lunar Exploration Neutron Detector (LEND). Icarus 255:100–115

Lucey PG (2009) The poles of the Moon. Elements 5:41–66

Lucey PG, Neumann GA, Riner MA, Mazarico E, Smith DE, Zuber MT, Paige DA, Bussey DBJ, Cahill JT, McGovern A, Isaacson P, Corley LM, Torrence MH, Melosh HJ, Head JW, Song E (2014) The global albedo of the Moon at 1064 nm from LOLA. J Geophys Res: Planets 119:1665–1679

Managadze GG, Cherepin VT, Shkuratov YG, Kolesnik VN, Chumikov AE (2011) Simulating OH/H_2O formation by solar wind at the lunar surface. Icarus 215:449–451

Mangano V, Massetti S, Milillo A, Mura A, Orsini S, Leblanc F (2013) Dynamical evolution of sodium anisotropies in the exosphere of Mercury. Planet Space Sci 82–83:1–10

Margot JL, Campbell DB, Jurgens RF, Slade MA (1999) Topography of the lunar poles from radar interferometry: A survey of cold trap locations. Science 284:1658–1660

Mattern PL, Thomas GJ, Bauer W (1976) Hydrogen and helium implantation in vitreous silica. J Vac Sci Technol 13:430

Matthewman R, Court RW, Crawford IA, Jones AP, Joy KH, Sephton MA (2015) The Moon as a recorder of organic evolution in the early solar system: a lunar regolith analog study. Astrobiol 15:154–168

Mazarico E, Neumann GA, Smith DE, Zuber MT, Torrence MH (2011) Illumination conditions of the lunar polar regions using LOLA topography. Icarus 211:1066–1081

McClanahan TP, Mitrofanov IG, Boynton WV, Chin G, Bodnarik J, Droege G, Evans LG, Golovin D, Hamara D, Harshman K, Litvak M, Livengood TA, Malakhov A, Mazarico E, Milikh G, Nandikotkur G, Parsons A, Sagdeev R, Sanin A, Starr RD, Su JJ, Murray J (2015) Evidence for the sequestration of hydrogen-bearing volatiles towards the Moon's southern pole-facing slopes. Icarus 255:88–99

McClintock WE, Bradley ET, Vervack RJ Jr., Killen RM, Sprague AL, Izenberg NR, Solomon SC (2008) Mercury's exosphere: observations during MESSENGER's First Mercury flyby. Science 321:92–94

McCord TB, Sotin C (2005) Ceres: Evolution and current state. J Geophys Res 110(E5):E05009

McCord TB, Taylor LA, Combe JP, Kramer GY, Pieters CM, Sunshine JM, Clark RN (2011) Sources and physical processes responsible for OH/H_2O in the lunar soil as revealed by the Moon Mineralogy Mapper (M3). J Geophys Res 116:E00G05

McCubbin FM, Kaaden KEV, Tartèse R, Klima RL, Liu Y, Mortimer J, Barnes JJ, Shearer CK, Treiman AH, Lawrence DJ, Elardo SM, Hurley DM, Boyce JW, Anand M (2015) Magmatic volatiles (H, C, N, F, S, Cl) in the lunar mantle, crust, and regolith: Abundances, distributions, processes, and reservoirs. Am Mineral 100:1668–1707

McCubbin FM, Barnes JJ, Ni P, Hui H, Klima RL, Burney D, Day JMD, Magna T, Boyce JW, Tartèse R, Vander Kaaden KE, Steenstra E, Elardo SM, Zeigler RA, Anand M, Liu Y (2023) Endogenous lunar volatiles. Rev Mineral Geochem 89:729–786

McGovern JA, Bussey DBJ, Greenhagen BT, Paige DA, Cahill JTS, Spudis PD (2013) Mapping and characterization of non-polar permanent shadows on the lunar surface. Icarus 223:566–581

McGuire RE, von Rosenvinge TT (1984) The energy spectra of solar energetic particles. Adv Space Res 4:117–125

Meyer FW, Harris PR, Taylor CN, Meyer III HM, Barghouty AF, Adams JH (2011) Sputtering of lunar regolith simulant by protons and singly and multicharged Ar ions at solar wind energies. Nucl Instrum Methods Phys Res Sect B 269:1316–1320

Miller RS, Nerurkar G, Lawrence DJ (2012) Enhanced hydrogen at the lunar poles: New insights from the detection of epithermal and fast neutron signatures. J Geophys Res 117:E11007

Miller RS, Lawrence DJ, Hurley DM (2014) Identification of surface hydrogen enhancements within the Moon's Shackleton crater. Icarus 233:229–232

Milliken RE, Li S (2017) Remote detection of widespread indigenous water in lunar pyroclastic deposits. Nat Geosci 10:561–565

Mitchell EH, Raut U, Fulvio D, Schaible MJ, Dukes CA, Baragiola RA (2013) Ultraviolet photodesorption as a driver of water migration on the lunar surface. Planet Space Sci 89:42–46

Mitrofanov IG, Sanin AB, Boynton WV, Chin G, Garvin JB, Golovin D, Evans LG, Harshman K, Kozyrev AS, Litvak ML, Malakhov A, Mazarico E, McClanahan T, Milikh G, Mokrousov M, Nandikotkur G, Neumann GA, Nuzhdin I, Sagdeev R, Shevchenko V, Shvetsov V, Smith DE, Starr R, Tretyakov VI, Trombka J, Usikov D, Varenikov A, Vostrukhin A, Zuber MT (2010) Hydrogen mapping of the lunar south pole using the LRO neutron detector experiment LEND. Science 330:483–486

Mitrofanov IG, Litvak M, Sanin A, Malakhov A, Golovin D, Boynton WV, Droege G, Chin G, Evans L, Harshman K, Fedosov F, Garvin J, Kozyrev A, McClanahan T, Milikh G, Mokrousov M, Starr R, Sagdeev R, Shevchenko V, Shvetsov V, Tret'yakov V, Trombka J, Varenikov A, Vostrukhin A (2012) Testing polar spots of water-rich permafrost on the Moon: LEND observations onboard LRO. J Geophys Res: Planets 117(E12):E00H27

Moores JE (2016) Lunar water migration in the interval between large impacts: Heterogeneous delivery to permanently shadowed regions, fractionation, and diffusive barriers. J Geophys Res: Planets 121:46–60

Morgan TH, Shemansky DE (1991) Limits to the lunar atmosphere. J Geophys Res 96(A2):1351–1367

Morris RV (1978) In situ reworking (gardening) of the lunar surface: Evidence from the Apollo cores. Proc Lunar Planet Sci Conf 9th:1801–1811

Nakajima M, Stevenson DJ (2018) Inefficient volatile loss from the Moon-forming disk: Reconciling the giant impact hypothesis and a wet Moon. Earth Planet Sci Lett 487:117–126

Needham DH, Kring DA (2017) Lunar volcanism produced a transient atmosphere around the ancient Moon. Earth Planet Sci Lett 478:175–178

Neish CD, Bussey DBJ, Spudis PD, Marshall W, Thomson BJ, Patterson GW, Carter LM (2011) The nature of lunar volatiles as revealed by Mini-RF observations of the LCROSS impact site. J Geophys Res 116(E1):E01005

Neumann GA, Cavanaugh JF, Sun X, Mazarico E, Smith DE, Zuber MT, Mao D, Paige DA, Solomon SC, Ernst CM, Barnouin OS (2013) Bright and dark polar deposits on Mercury: Evidence for surface volatiles. Science 339:296

Nozette S, Lichtenberg CL, Spudis PD, Bonner R, Ort W, Malaret E, Robinson MS, Shoemaker EM (1996) The Clementine bistatic radar experiment. Science 274:1495–1498

Ong L, Asphaug EI, Korycansky D, Coker RF (2010) Volatile retention from cometary impacts on the Moon. Icarus 207:578–589

Paige DA, Wood SE, Vasavada AR (1992) The thermal stability of water ice at the poles of Mercury. Science 258:643–646

Paige DA, Siegler MA, Zhang JA, Hayne PO, Foote EJ, Bennett KA, Vasavada AR, Greenhagen BT, Schofield JT, McCleese DJ, Foote MC, DeJong E, Bills BG, Hartford W, Murray BC, Allen CC, Snook K, Soderblom LA, Calcutt S, Taylor FW, Bowles NE, Bandfield JL, Elphic RC, Ghent R, Glotch TD, Wyatt MB, Lucey PG (2010) Diviner lunar radiometer observations of cold traps in the Moon's south polar region. Science 330:479–482

Paige DA, Siegler MA, Harmon JK, Neumann GA, Mazarico EM, Smith DE, Zuber MJKT, Harju E, Delitsky ML, Solomon SC (2013) Thermal stability of volatiles in the north polar region of Mercury. Science 339:300–303

Patterson GW, Stickle AM, Turner FS, Jensen JR, Bussey DBJ, Spudis PD, Espiritu RC, Schulze RC, Yocky DA, Wahl DE, Zimmerman M, Cahill JTS, Nolan M, Carter L, Neish CD, Raney RK, Thomson BJ, Kirk R, Thompson TW, Tise BL, Erteza IA, Jakowatz CV (2017) Bistatic radar observations of the Moon using Mini-RF on LRO and the Arecibo Observatory. Icarus 283:2–19

Pierazzo E, Melosh HJ (2000) Hydrocode modeling of oblique impacts: The fate of the projectile. Meteorit Planet Sci 35:117–130

Pieters CM, Goswami JN, Clark RN, Annadurai M, Boardman J, Buratti B, Combe JP, Dyar MD, Green R, Head JW, Hibbitts CA, Hicks M, Isaacson P, Klima R, Kramer G, Kumar S, Livo E, Lundeen S, Malaret E, McCord T, Mustard J, Nettles J, Petro N, Runyon C, Staid M, Sunshine J, Taylor LA, Tompkins S, Varanasi P (2009) Character and spatial distribution of OH/H_2O on the surface of the Moon seen by M3 on Chandrayaan-1. Science 326:568–572

Platz T, Nathues A, Schorghofer N, Preusker F, Mazarico E, Schröder SE, Byrne S, Kneissl T, Schmedemann N, Combe JP, Schäfer M, Thangjam GS, Hoffmann M, Gutierrez-Marques P, Landis ME, Dietrich W, Ripken J, Mantz KD, Russell CT (2016) Surface water-ice deposits in the northern shadowed regions of Ceres. Nat Astron 1:7

Poppe AR, Halekas JS, Lue C, Fatemi S (2017) ARTEMIS observations of the solar wind proton scattering function from lunar crustal magnetic anomalies. J Geophys Res: Planets 122:771–783

Poston MJ, Grieves GA, Aleksandrov AB, Hibbitts CA, Dyar MD, Orlando TM (2013) Water interactions with micronized lunar surrogates JSC-1A and albite under ultra-high vacuum with application to lunar observations. J Geophys Res: Planets 118:105–115

Poston MJ, Grieves GA, Aleksandrov AB, Hibbitts CA, Dyar MD, Orlando TM (2015) Temperature programmed desorption studies of water interactions with Apollo lunar samples 12001 and 72501. Icarus 255:24–29
Prem P, Artemieva NA, Goldstein DB, Varghese PL, Trafton LM (2015) Transport of water in a transient impact-generated lunar atmosphere. Icarus 255:148–158
Reed GWJ (1999) Don't drink the water. Meteorit Planet Sci 34:809–811
Rubanenko L, Aharonson O (2017) Stability of ice on the Moon with rough topography. Icarus 296:99–109
Russell CT, Raymond CA (2011) The Dawn mission to Vesta and Ceres. Space Sci Rev 163:3–23
Saal AE, Hauri EH, Cascio ML, Van Orman JA, Rutherford MJ, Cooper RF (2008) Volatile content of lunar volcanic glasses and the presence of water in the Moon's interior. Nature 454:192–195
Saal AE, Hauri EH, Van Orman JA, Rutherford MJ (2013) Hydrogen isotopes in lunar volcanic glasses and melt inclusions reveal a carbonaceous chondrite heritage. Science 340:1317–1320
Sacksteder KR, Sanders GB (2007) In situ resource utilization for lunar and Mars exploration. 45th AIAA Aerospace Sciences Meeting and Exhibit
Saito Y, Yokota S, Tanaka T, Asamura K, Nishino MN, Fujimoto M, Tsunakawa H, Shibuya H, Matsushima M, Shimizu H, Takahashi F, Mukai T, Terasawa T (2008) Solar wind proton reflection at the lunar surface: Low energy ion measurement by MAP-PACE onboard SELENE (KAGUYA). Geophys Res Lett 35:L24205
Sanders GB, Larson WE (2015) Final review of analog field campaigns for in situ resource utilization technology and capability maturation. Adv Space Res 55:2381–2404
Sanin AB, Mitrofanov IG, Litvak ML, Bakhtin BN, Bodnarik JG, Boynton WV, Chin G, Evans LG, Harshman K, Fedosov F, Golovin DV, Kozyrev AS, Livengood TA, Malakhov AV, McClanahan TP, Mokrousov MI, Starr RD, Sagdeev RZ, Tret'yakov VI, Vostrukhin AA (2017) Hydrogen distribution in the lunar polar regions. Icarus 283:20–30
Sarantos M, Killen RM, Surjalal Sharma A, Slavin JA (2010) Sources of sodium in the lunar exosphere: Modeling using ground-based observations of sodium emission and spacecraft data of the plasma. Icarus 205:364–374
Schaible MJ, Baragiola RA (2014) Hydrogen implantation silicates: The role of solar wind in SiOH bond formation on the surfaces of airless bodies in space, J Geophys Res 119:2017–2028
Schaible MJ, Johnson RE, Zhigilei LV, Piqueux S (2017) High energy electron sintering of icy regoliths: Formation of the PacMan thermal anomalies on the icy Saturnian moons. Icarus 285:211–223
Schwadron NA, Wilson JK, Jordan AP, Looper MD, Zeitlin C, Townsend LW, Spence HE, Legere J, Bloser P, Farrell WM, Hurley DM, Petro N, Stubbs TJ, Pieters CM (2018) Using proton radiation from the moon to search for diurnal variation of regolith hydrogenation. Planet Space Sci 162:113–132
Schorghofer N, Aharonson O (2014) The lunar thermal ice pump. Astrophys J 788:169
Schorghofer N, Taylor GJ (2007) Subsurface migration of H_2O at lunar cold traps. J Geophys Res 112(E2):E02010
Schorghofer N, Mazarico E, Platz T, Preusker F, Schröder SE, Raymond CA, Russell CT (2016) The permanently shadowed regions of dwarf planet Ceres. Geophys Res Lett 43:6783– 6789
Schorghofer N, Lucey PG, Williams J-P (2017) Theoretical time variability of mobile water on the Moon and its geographic pattern. Icarus 298:111–116
Schwadron NA, Baker T, Blake B, Case AW, Cooper JF, Golightly M, Jordan A, Joyce C, Kasper J, Kozarev K, Mislinski J, Mazur J, Posner A, Rother O, Smith S, Spence HE, Townsend LW, Wilson J, Zeitlin C (2012) Lunar radiation environment and space weathering from the Cosmic Ray Telescope for the Effects of Radiation (CRaTER). J Geophys Res: Planets 117(E12):E00H13
Schwadron NA, Wilson JK, Jordan AP, Looper MD, Zeitlin C, Townsend LW, Spence HE, Legere J, Bloser P, Farrell WM, Hurley DM, Petro N, Stubbs TJ, Pieters CM (2016) Using proton radiation from the Moon to search for diurnal variation of regolith hydrogenation. Planet Space Sci 162:113–132
Siegler MA, Paige DA, Williams J-P, Bills B (2015) Evolution of lunar polar ice stability. Icarus 255:78–87
Siegler MA, Bills BG, Paige DA (2011) Effects of orbital evolution on lunar ice stability. J Geophys Res 116(E3):E03010
Siegler MA, Miller RS, Keane JT, Laneuville M, Paige DA, Matsuyama I, Lawrence DJ, Crotts A, Poston MJ (2016) Lunar true polar wander inferred from polar hydrogen. Nature 531:480–484
Sim CK, Kim SS, Lucey PG, Garrick-Bethell I, Choi Y-J (2017) Asymmetric space weathering on lunar crater walls. Geophys Res Lett 44:11,273–211,281
Simpson RA, Tyler GL (1999) Reanalysis of Clementine bistatic radar data from the lunar South Pole. J Geophys Res: Planets 104(E2):3845–3862
Slade MA, Butler BJ, Muhleman DO (1992) Mercury radar imaging: evidence for polar ice. Science 258:635–640
Smart DF, Shea MA (1985) Galactic cosmic radiation and solar energetic particles. *In:* Handbook of Geophysics and the Space Environment. Jura AS (ed). Bedford, MA, Air Force Geophysics Laboratory, p 6-1–6-29
Spudis PD, Bussey DBJ, Baloga SM, Butler BJ, Carl D, Carter LM, Chakraborty M, Elphic RC, Gillis-Davis JJ, Goswami JN, Heggy E, Hillyard M, Jensen R, Kirk RL, LaVallee D, McKerracher P, Neish CD, Nozette S, Nylund S, Palsetia M, Patterson GW, Robinson MS, Raney RK, Schulze RC, Sequeira H, Skura J, Thompson TW, Thomson BJ, Ustinov EA, Winters HL (2010) Initial results for the north pole of the Moon from Mini-SAR, Chandrayaan-1 mission. Geophys Res Lett 37:L06204
Spudis PD, Bussey DBJ, Baloga SM, Cahill JTS, Glaze LS, Patterson GW, Raney RK, Thompson TW, Thomson BJ, Ustinov EA (2013) Evidence for water ice on the Moon: Results for anomalous polar craters from the LRO Mini-RF imaging radar. J Geophys Res: Planets 118:2016–2029

Stacy NJS, Campbell DB, Ford PG (1997) Arecibo radar mapping of the lunar poles: A search for ice deposits. Science 276:1527–1530
Starukhina L (2001) Water detection of atmosphereless celestial bodies: Alternative explanations of the observations. J Geophys Res 106(E7):14,701–14,710
Starukhina L (2003) Computer simulation of sputtering of lunar regolith by solar wind protons: Contribution to change of surface composition and to hydrogen flux and the lunar poles. Sol Sys Res 37:36–50
Starukhina L (2006) Polar regions of the moon as a potential repository of solar-wind-implanted gases. Adv Space Res 37:50–58
Starukhina L (2012) Water on the Moon: What is derived from the observations? Chapter 3 *In:* Moon, Springer, p 57–85
Starukhina LV, Shkuratov YG (2000) The lunar poles: Water ice or chemically trapped hydrogen? Icarus 147:585–587
Stern SA, Cook JC, Chaufray JY, Feldman PD, Gladstone GR, Retherford KD (2013) Lunar atmospheric H_2 detections by the LAMP UV spectrograph on the Lunar Reconnaissance Orbiter. Icarus 226:1210–1213
Stewart BD, Pierazzo E, Goldstein DB, Varghese PL, Trafton LM (2011) Simulations of a comet impact on the Moon and associated ice deposition in polar cold traps. Icarus 215:1–16
Sunshine JM, Farnham TL, Feaga LM, Groussin O, Merlin F, Milliken RE, A'Hearn MF (2009) Temporal and spatial variability of lunar hydration as observed by the Deep Impact spacecraft. Science 326:565–568
Svetsov VV, Shuvalov VV (2015) Water delivery to the Moon by asteroidal and cometary impacts. Planet Space Sci 117:444–452
Syal MB, Schultz PH, Riner MA (2015) Darkening of Mercury's surface by cometary carbon. Nat Geosci 8:352–356
Szalay JR, Horányi M (2015) Annual variation and synodic modulation of the sporadic meteoroid flux to the Moon. Geophys Res Lett 42:10,580–510,584
Tenishev V, Rubin M, Tucker OJ, Combi MR, Sarantos M (2013) Kinetic modeling of sodium in the lunar exosphere. Icarus 226:1538–1549
Thomson BJ, Bussey DBJ, Neish CD, Cahill JTS, Heggy E, Kirk RL, Patterson GW, Raney RK, Spudis PD, Thompson TW, Ustinov EA (2012) An upper limit for ice in Shackleton crater as revealed by LRO Mini-RF orbital radar. Geophys Res Lett 39:L14201
Tucker OJ, Farrell WM, Killen RM, Hurley DM (2019) Solar wind implantation into the lunar regolith: Monte Carlo simulations of H retention in a surface with defects and the H_2 exosphere. J Geophys Res: Planets 124:278– 293
Urey HC (1952) The Planets: Their Origin and Development. New Haven, Yale University Press
Vasavada AR, Paige DA, Wood SE (1999) Near-surface temperatures on Mercury and the Moon and the stability of polar ice deposits. Icarus 141:179–193
Vondrak R, Crider D (2003) Ice at the lunar poles—That the moon harbors ice at high latitudes is well known. The source of that water, however, may come as something of a surprise. Am Sci 91:322–329
Vondrak RR (1974) Creation of an artificial lunar atmosphere. Nature 248:657–659
Ward WR (1975) Past orientation of the lunar spin axis. Science 189:377–379
Watson K, Murray BC, Brown H (1961) The behavior of volatiles on the lunar surface. J Geophys Res 66:3033–3052
Wieser M, Barabash S, Futaana Y, Holmström M, Bhardwaj A, Sridharan R, Dhanya MB, Schaufelberger A, Wurz P, Asamura K (2010) First observation of a mini-magnetosphere above a lunar magnetic anomaly using energetic neutral atoms. Geophys Res Lett 37:L05103
Wieser M, Barabash S, Futaana Y, Holmström M, Bhardwaj A, Sridharan R, Dhanya MB, Wurz P, Schaufelberger A, Asamura K (2009) Extremely high reflection of solar wind protons as neutral hydrogen atoms from regolith in space. Planet Space Sci 57:2132–2134
Williams JP, Paige DA, Greenhagen BT, Sefton-Nash E (2017) The global surface temperatures of the Moon as measured by the Diviner Lunar Radiometer Experiment. Icarus 283:300–325
Wilson JK, Baumgardner J, Mendillo M (2003) The outer limits of the lunar sodium exosphere. Geophys Res Lett 30:1649
Wilson JK, Mendillo M, Spence HE (2006) Magnetospheric influence on the Moon's exosphere. J Geophys Res 111(A7):A07207
Wilson JT, Lawrence DJ, Peplowski PN, Cahill JTS, Eke VR, Massey RJ, Teodoro LFA (2018) Image reconstruction techniques in neutron and gamma ray spectroscopy: Improving Lunar Prospector Data. J Geophys Res: Planets 123:1804–1822
Wöhler C, Grumpe A, Berezhnoy AA, Feoktistova EA, Evdokimova NA, Kapoor K, Shevchenko VV (2017) Temperature regime and water/hydroxyl behavior in the crater Boguslawsky on the Moon. Icarus 285:118–136
Yamamoto T (1985) Formation environment of cometary nuclei in the primordial solar nebula. Astron Astrophys 142:31–36
Zeller EJ, Ronca LB, Levy PW (1966) Proton-induced hydroxyl formation on the lunar surface. J Geophys Res 71:4855–4860
Zhang JA, Paige DA (2009) Cold-trapped organic compounds at the poles of the Moon and Mercury: Implications for origins. Geophys Res Lett 36:L16203
Zimmerman MI, Jackson TL, Farrell WM, Stubbs TJ (2012) Plasma wake simulations and object charging in a shadowed lunar crater during a solar storm. J Geophys Res: Planets 117(E10):E00K03
Zuber MT, Head JW, Smith DE, Neumann GA, Mazarico E, Torrence MH, Aharonson O, Tye AR, Fassett CI, Rosenburg MA, Melosh HJ (2012) Constraints on the volatile distribution within Shackleton crater at the lunar south pole. Nature 486:378–381

APPENDIX—RECENT DEVELOPMENTS

A recent re-analysis of the LCROSS plume observations has been conducted by Mandt et al. (2022). Rather than using molecular compositions, they instead examined elemental composition ratios and compared the ratios to various possible sources. Losses over time were also examined. They determined that the volatiles from the crater floor are likely not volcanic in origin. Instead, ratios better fit an exogenic cometary source.

H_2O exhibits a spectral emission feature at 6 μm that does not occur in OH. Thus, observations of the Moon at 6 μm have provided an additional viewpoint of water adsorbed to the illuminated surface of the Moon that can distinguish between OH and H_2O. Honniball et al. (2021) use the NASA/DLR Stratospheric Observatory for Infrared Astronomy (SOFIA) to reveal water (H_2O) in abundances of 100–400 μg/g at high latitudes that are consistent with water stored within glasses or voids between regolith grains.

Lin et al. (2022) report the first in situ detection of H_2O/OH on the surface of the Moon using the Lunar Mineralogical Spectrometer (LMS) on the Chang'e 5 lander. In the vicinity of the Chang'e 5 landing site in northern Oceanus Procellarum the data are consistent with the regolith being primarily devoid of OH/H_2O. However, some locations of regolith contained up to 120 ppm of OH/H_2O, potentially preserved from removal by the landing plume due to shielding by rocks. In addition, one rock (CE5-Rock) appears to contain ~180 ppm of OH/H_2O and is consistent with water retained from the lunar interior.

New modeling tools have been developed to predict the global exospheric and surface effects of a lunar lander plume. Prem et al. (2020) found that there are possible global consequences of a landing at high latitudes, with a relatively large fraction of the plume water vapor possibly being capable of migrating into the lunar cold traps, contaminating the pristine materials trapped within. This work was heavily cited by the National Academy's Committee on Planetary Protection (2020), which noted that there is a lack of studies characterizing the level of contamination of volatiles that would be harmful to future science investigations of PSR chemical evolution.

REFERENCES

Honniball CI, Lucey PG, Li S, Shenoy S, Orlando T, Hibbitts CA, Hurley DM, Farrell WM (2021) Molecular water detected on the sunlit Moon by SOFIA. Nat Astron 5:121–127

Lin H, S. Li S, Xu R, Liu U, Wu X, Yang W, Wei Y, Lin Y, He Z, Hui H, He H, Hu S, Zhang C, Li C, Lv F, Yuan L, Zou Y, Wang C (2022) In situ detection of water on the Moon by the Chang'E 5 lander. Sci Adv 8:eabl9174

Mandt KE, Mousis O, Hurley D, Bouquet A, Retherford KD, Magana LO, Luspay-Kuti A (2022) Exogenic origin for the volatiles sampled by the Lunar Crater Observation and Sensing Satellite impact. Nat Commun 13:642

National Academies Committee on Planetary Protection (2020) Planetary protection for the study of lunar volatiles. Nat Acad Press https://doi.org/10.17226/26029

Prem P, Hurley DM, Goldstein DB, Varghese PL (2020) The evolution of a spacecraft-generated lunar exosphere. J Geophys Res: Planets 125:e2020JE006464